



HAL
open science

Dynamic sensitivity analysis of a mathematical model describing the effect of the macroalgae *Asparagopsis taxiformis* on rumen fermentation and methane production under in vitro continuous conditions

Paul Blondiaux, Tristan Senga Kiessé, Maguy Eugène, Rafael Muñoz-Tamayo

► To cite this version:

Paul Blondiaux, Tristan Senga Kiessé, Maguy Eugène, Rafael Muñoz-Tamayo. Dynamic sensitivity analysis of a mathematical model describing the effect of the macroalgae *Asparagopsis taxiformis* on rumen fermentation and methane production under in vitro continuous conditions. 2024. hal-04628905

HAL Id: hal-04628905

<https://hal.science/hal-04628905>

Preprint submitted on 28 Jun 2024

HAL is a multi-disciplinary open access archive for the deposit and dissemination of scientific research documents, whether they are published or not. The documents may come from teaching and research institutions in France or abroad, or from public or private research centers.

L'archive ouverte pluridisciplinaire **HAL**, est destinée au dépôt et à la diffusion de documents scientifiques de niveau recherche, publiés ou non, émanant des établissements d'enseignement et de recherche français ou étrangers, des laboratoires publics ou privés.

RESEARCH ARTICLE



Open Access



Open Data



Open Code

*Correspondence:
paul.blondiaux@inrae.fr

Dynamic sensitivity analysis of a mathematical model describing the effect of the macroalgae *Asparagopsis taxiformis* on rumen fermentation and methane production under *in vitro* continuous conditions

Paul Blondiaux^{1*} , Tristan Senga Kiessé² , Maguy Eugène³  and Rafael Muñoz-Tamayo¹ 

¹ Université Paris-Saclay, INRAE, AgroParisTech, UMR Modélisation Systémique Appliquée aux Ruminants, 91120, Palaiseau, France.

² INRAE, UMR SAS, Institut Agro, 35000 Rennes, France.

³ INRAE, UCA, VetAgro Sup, UMR Herbivores 1213, 63122 Saint-Genès-Champanelle, France.

Abstract

Ruminants plays an important role in global warming by emitting enteric methane (CH₄) through the degradation of feeds by the rumen microbiota. To better understand the dynamics fermentation outputs, including methane and volatile fatty acids (VFA) production, mathematical models have been developed. Sensitivity analysis (SA) methods quantify the contribution of model input parameters (IP) to the variation of an output variable of interest. In animal science, SA are usually conducted in static condition. In this work, we hypothesized that including the dynamic aspect of the rumen fermentation to SA can be useful to inform on optimal experimental conditions aimed at quantifying the key mechanisms driving CH₄ and VFA production. Accordingly, the objective of this work was to conduct a dynamic SA of a rumen fermentation model under *in vitro* continuous conditions (close to the real *in vivo* conditions). Our model case study integrates the effect of the macroalgae *Asparagopsis taxiformis* (AT) on the fermentation. AT has been identified as a potent CH₄ inhibitor via the presence of bromoform, an anti-methanogenic compound. We implemented two SA methods. We computed Shapley effects and full and independent Sobol indices over time for quantifying the contribution of 16 IPs to CH₄ (mol/h) and VFA (mol/l) variation. Our approach allows to discriminate the 3 contribution types of an IP to output variable variation (individual, via the interactions and via the dependence/correlation). We studied three diet scenarios accounting for several doses of AT relative to Dry Matter (DM): control (0% DM of AT), low treatment (LT: 0.25% DM of AT) and high treatment (HT: 0.50% DM of AT). Shapley effects revealed that hydrogen (H₂) utilizers microbial group via its Monod H₂ affinity constant highly contributed (> 50%) to CH₄ variation with a constant dynamic over time for control and LT. A shift on the impact of microbial pathways driving CH₄ variation was revealed for HT. IPs associated with the kinetic of bromoform utilization and with the factor modeling the direct effect of bromoform on methanogenesis were identified as influential on CH₄ variation in the middle of fermentation. Whereas, VFA variation for the 3 diet scenarios was mainly explained by the kinetic of fibers degradation, showing a high constant contribution (> 30%) over time. In addition, the Sobol indices indicated that interactions between IPs played a role on CH₄ variation, which was not the case of VFA variation. However, these results are dependent on the way interactions are represented in the model. The simulations computed for the SA were also used to analyze prediction uncertainty. It was related to the dynamic of dry matter intake (DMI, g/h), increasing during the high intake activity periods and decreasing when the intake activity was low. Moreover, CH₄ (mol/h) simulations showed a larger variability than VFA simulations, suggesting that the reduction of the uncertainty of IPs describing the activity of the H₂ utilizers microbial group is a promising lead to reduce the overall model uncertainty. Our results highlighted the dynamic nature of the influence of metabolic pathways on CH₄ productions under an anti-methanogenic treatment. SA tools can be further exploited to design optimal experiments studying rumen fermentation and CH₄ mitigation strategies. These optimal experiments would be useful to build robust models that can guide the development of sustainable nutrition strategies.

1 Introduction

2 Reducing methane (CH₄) emissions from ruminants is an important challenge for the livestock
3 sector. At the global level, these emissions are responsible of 14.5% of total greenhouse gases
4 (GHG) from human activity sources (Fao, 2017), highlighting the important role of ruminants
5 in global warming. In France, CH₄ emissions represented 48% of total GHG emissions from
6 agricultural sector in 2021 (CITEPA, 2023). In this context, Masson-Delmotte et al. (2019)
7 highlighted that decreasing agricultural CH₄ emissions by 11 to 30% of the 2010 level by 2030
8 and by 24 to 47% by 2050 must be achieved to meet the 1.5 °C target of the Paris Agreement.
9 In addition, Arndt et al. (2022) indicated that some mitigation strategies scenarios may allow
10 to meet the 1.5 °C target by 2030. However, this study also highlighted that it was not possible
11 to meet this target by 2050 considering that expected increase in milk and meat demand will
12 lead to an increase of GHG emissions.

13 Ruminants produce CH₄ during the degradation and fermentation of feeds (Morgavi et al.,
14 2010; Beauchemin et al., 2020). The fermentation process is done by a complex community
15 of microbes inhabiting the forestomach (rumen) of ruminants. These microbial community
16 (rumen microbiota) are constituted by members of bacteria, archaea, fungi and protozoa. The
17 products of fermentation include volatile fatty acids (VFA), which are useful compounds for
18 the animal, and CH₄. The development of mitigation actions aiming to reduce the enteric CH₄
19 production without affecting animal performance and welfare is a crucial challenge for the
20 field (Hristov et al., 2013; Pellerin et al., 2013; Torres et al., 2020).

21 To better understand rumen fermentation and help design such strategies, mechanistic
22 models describing the dynamic process of the rumen fermentation were developed. A
23 synthesis of the characteristics of these models is presented by Tedeschi et al. (2014). Among
24 these, the 3 most popular dynamic mechanistic models of rumen fermentation are: Molly
25 (Baldwin et al., 1987), Dijkstra et al. (1992) and Karoline (Danfær et al., 2006).

26 These dynamic models involved numerous input parameters (IPs) representing biological and
27 physical processes. The complexity of such models raises the need to investigate model
28 behaviour, including the various relationships among IPs and outputs. To address this need,
29 sensitivity analysis (SA) methods were used to assess the contribution of IP variability on the
30 variability of the output of interest, identifying IPs which contribute the most to model
31 predictions variability from those having a negligible effect (Faivre et al., 2013; looss and
32 Lemaître, 2015; Saltelli et al., 2008, 2005).

33 In animal science, SA is usually conducted on mechanistic models with the main objective of
34 reducing their complexity and identifying which IPs requires more accurate measurements for
35 reducing output uncertainty. For instance, Huhtanen et al. (2015) and van Lingen et al. (2019)
36 used linear regressions for describing the effects of some parameters on the variation of daily
37 scale enteric CH₄ emissions in the Karoline model and an updated version of the Dijkstra
38 model, respectively. In addition, Morales et al. (2021) and Dougherty et al. (2017) computed
39 the Sobol indices (Sobol, 1993) for quantifying the effects of 19 and 20 parameters on several
40 output variables of the Molly and AusBeef (Nagorcka et al., 2000) models, respectively.

41 Morales et al. (2021) did not consider the CH₄ production among the 27 output variables
42 studied, while VFAs were considered. Dougherty et al. (2017) considered the daily CH₄
43 production in the output variables. In both studies, uniform distributions were set for
44 exploring parameter variability. Recently, Merk et al. (2023) adapted and calibrated the model
45 of Muñoz-Tamayo et al. (2021) to represent experimental data from the *in vitro* RUSITEC study
46 of Roque et al. (2019), which aimed at evaluating the effect of the macroalgae *Asparagopsis*
47 *taxiformis* (AT) on CH₄ production and rumen microbiota. Authors used a Sobol based
48 approach for identifying key parameters associated to microbial pathways driving CH₄
49 production with and without the presence of AT.

50 Although different SA approaches were applied to mechanistic models in the literature,
51 several aspects still need to be explored. One aspect is the dynamic characteristic of the rumen
52 fermentation. Most of the studies mentioned above explored sensitivity of mechanistic
53 models at a single time point or under steady state conditions. However, the impact of IPs
54 might vary over time, since the rumen is a dynamic system. Capturing this dynamic effect is of
55 relevance to better understand rumen function (Morgavi et al., 2023) and to design CH₄
56 mitigation strategies. To our knowledge, SA has not been applied in dynamic conditions for
57 studying CH₄ and VFA predictions of rumen models. Other aspect to explore in mechanistic
58 models is the nature of the contribution of the IPs to model outputs by identifying: 1) the
59 effect due to the IPs alone, 2) the effect due to the interactions between the IPs and 3) the
60 effect due to the dependence or correlation between the IPs. Some references mentioned
61 above implemented a method differentiating some effects of the contribution of an IP to
62 output (individual, interaction and dependence/correlation). Dougherty et al. (2017)
63 computed first-order and total Sobol indices (Homma and Saltelli, 1996), quantifying the
64 individual and interaction effects of IPs. Whereas, van Lingen et al. (2019) concluded that
65 there was no interaction between parameter covariates when studying the variation of daily
66 scale enteric CH₄ emissions. The quantification of the contribution due to the
67 dependence/correlation between the IPs has been an important research activity of the
68 applied mathematics field for several years now (Kucherenko et al., 2012; Mara et al., 2015;
69 Xu and Zdzislaw Gertner, 2008). Not all the SA methods are able to identify these 3 effects,
70 conducting to biases in the estimated sensitivity indices.

71 The aim of this work was to conduct a complete SA of a dynamic model of rumen fermentation
72 under *in vitro* continuous conditions accounting for the effect of AT on the fermentation and
73 CH₄ production. The model studied extends previous developments of Muñoz-Tamayo et al.
74 (2016, 2021). The AT macroalgae has been identified as a potent CH₄ inhibitor (Machado et
75 al., 2014) with reported *in vivo* reductions of CH₄ emissions over 80% and 98% in beef cattle
76 (Kinley et al., 2020; Roque et al., 2021). The original model (Muñoz-Tamayo et al., 2021)
77 represented the fermentation under batch conditions. We extended the model to account for
78 continuous condition which aimed at providing a model closer to the *in vivo* conditions. Also,
79 the *in silico* framework in which SA is conducted was used to analyze the uncertainty
80 associated with the outputs of interest over time. This work also addresses the limitations
81 pointed out by Tedeschi (2021) in the evaluation process of the model in Muñoz-Tamayo et

82 al. (2021), which did not include SA to assess the impact of model parameters on the model
83 outputs.

84 2. Methods

85 2.1. Presentation of the mechanistic model

86 2.1.1. Phenomena representation

87 The structure of the rumen fermentation model used in this study is determined by the
88 representation of two phenomena namely the flow transport and microbial fermentation. The
89 first is a biochemical and physical phenomenon describing the transport fluxes in the system,
90 here represented as a reactor. The second is a biological phenomenon describing the
91 microbial fermentation of feeds.

92 The system studied is displayed in Figure 1.

93

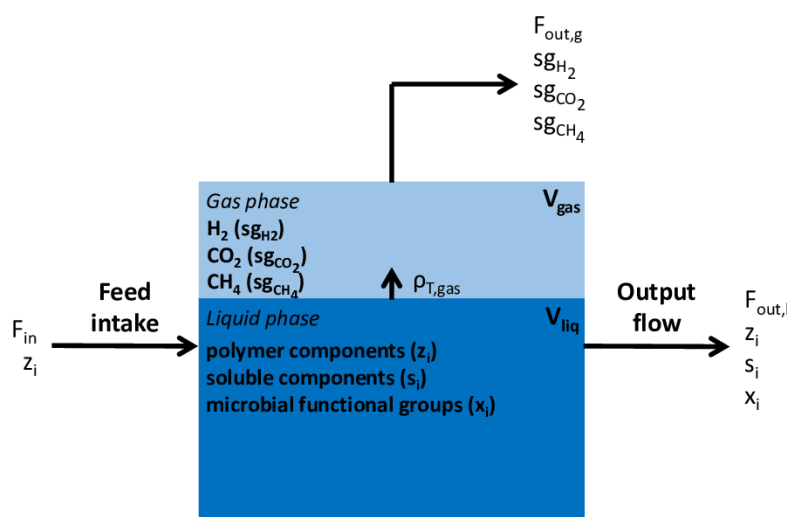


Figure 1. Representation of the *in vitro* continuous system.

94

95 This system is represented as a reactor system similar to engineering anaerobic digestion
96 reactors (Batstone et al., 2002). It represents a rumen simulation technique (RUSITEC) system
97 on a daily scale. Characteristics of the simulated RUSITEC system were taken from the setting
98 used in Belanche et al., 2017. The total volume of the system was set to 0.8 L with a separation
99 of 0.74 L in liquid phase (V_l) and 0.06 L in gas phase (V_g). The daily total dry matter intake (DMI)
100 was of 11.25 g/d. In our model, the DMI was set as a dynamic equation determined by the
101 number of feed distributions (n_r). For the feed distribution j , the DMI kinetics follows

$$102 \quad DMI(t) = \frac{\lambda_{n_j} \cdot DM_{total}}{n_r} \cdot e^{-kt} \quad (1)$$

103 Where DM_{total} is the total DMI ingested in one day (g), λ_{n_j} is the fraction of DM_{total} supplied
104 in the distribution j and k (h^{-1}) is the intake kinetic rate. DM_{total} was set to 11.25 g supplied
105 in two feed distributions ($n_r = 2$). We set the first feed distribution to account for 70% of the

106 total DM ($\lambda_{n_1} = 0.7$). This configuration provides a daily DMI composed of 2 distributions
 107 with a significantly greater amount of dry matter (DM) ingested during the first intake and a
 108 medium intake kinetic (Figure 2).
 109

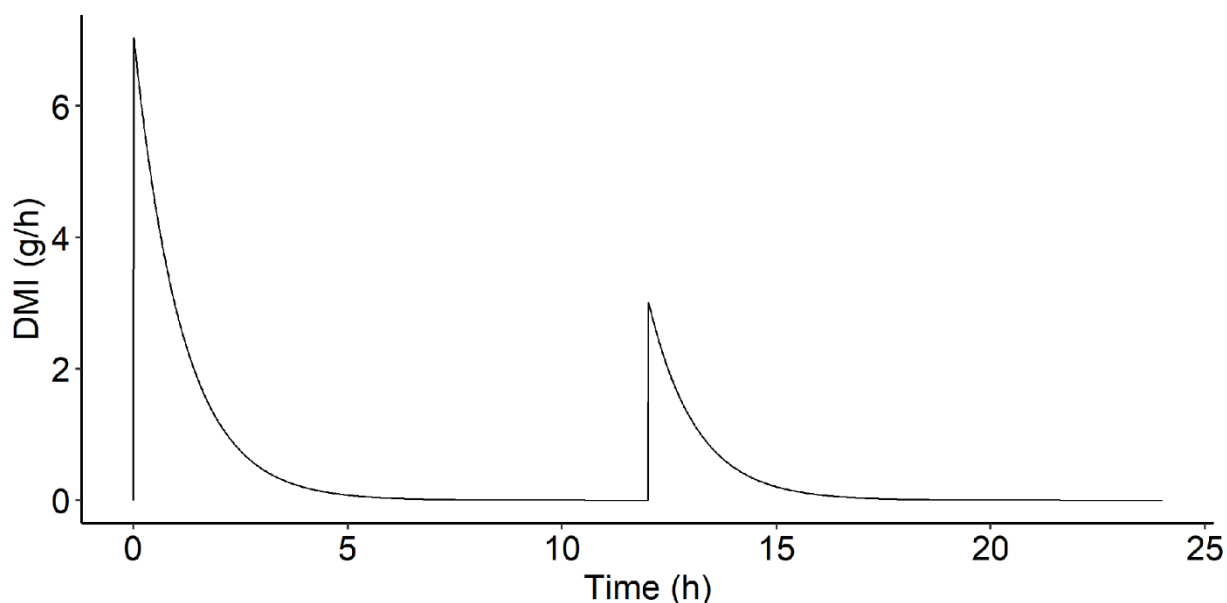


Figure 2. Dry matter intake (DMI, g/h) over time (h) simulated for one day with $DM_{total} = 11.25$ g, $n_r = 2$, $\lambda_{n_1} = 0.7$ and $k = 0.015$.

110
 111 The feed intake constitutes the input flux of the system. The feed is degraded by the rumen
 112 microbiota, leading to the production of several components in liquid and gas phase. Polymer
 113 components, soluble components and microbial functional groups are the components in
 114 liquid phase, and hydrogen, carbon dioxide and CH_4 are the components in gas phase.
 115 Chemical compounds leave the system in liquid and gas phases as shown in Figure 1.
 116 The representation of the fermentation process is displayed in Figure 3.
 117

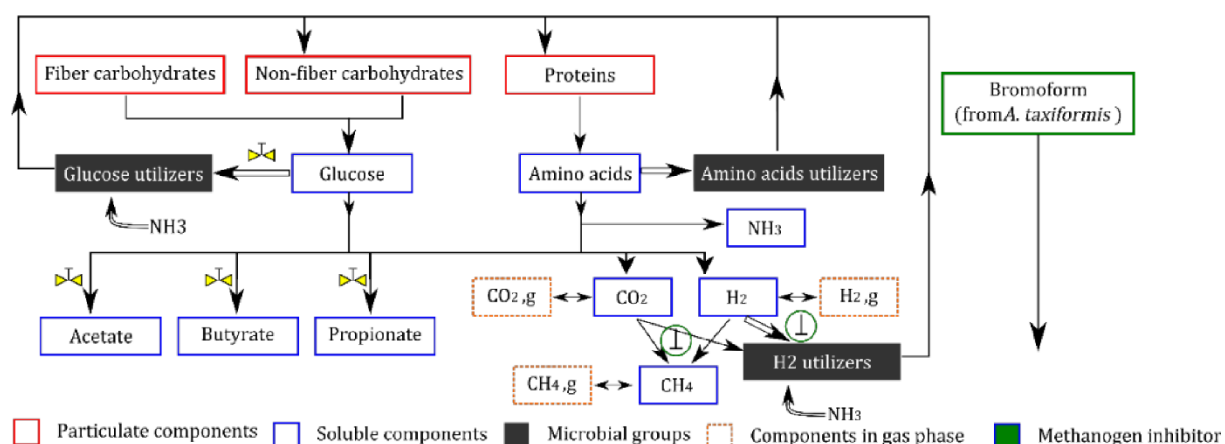


Figure 3. Representation of the *in vitro* rumen fermentation from Muñoz-Tamayo et al., 2021 model.

118

119 Biochemical assumptions used to describe the fermentation are detailed in Muñoz-Tamayo et
120 al. (2021, 2016). The main assumptions are: 1) 3 polymer components are considered in the
121 rumen: fiber carbohydrates, non-fiber carbohydrates and proteins, 2) hydrolysis of polymer
122 components releases glucose (for fibers and non-fibers) and amino acids (for proteins),
123 constituting 2 of the 3 soluble limiting substrates available in the rumen. The last soluble
124 limiting substrate available is hydrogen, 3) the rumen microbiota is represented by 3 microbial
125 functional groups (glucose utilizers, amino acids utilizers and hydrogen utilizers) determined
126 by the microbial utilization of the 3 soluble limiting substrates in the fermentation pathway,
127 4) the utilization of the soluble substrates by biological pathways is done towards 2
128 mechanisms: product formation and microbial growth, 5) acetate, propionate and butyrate
129 are the only VFA produced from the fermentation and 6) CH₄, carbon dioxide and hydrogen
130 are the gas outputs of the fermentation.

131 The inclusion of bromoform as the inhibitor compound of AT impacted the fermentation *via*
132 2 mechanisms. First, the bromoform has a direct inhibition of the growth rate of
133 methanogens, resulting in a CH₄ production reduction and hydrogen accumulation. Second,
134 the bromoform affects indirectly, through the hydrogen accumulation, the flux allocation
135 towards VFA production, as hydrogen exerts control on this component (Mosey, 1983).

136 The resulting model comprises 19 state variables corresponding to 19 biochemical component
137 concentrations in liquid and gas phases.

138 2.1.2. Model equations

139 Model state variables are defined as $\xi = (\mathbf{z}, \mathbf{s}, \mathbf{x}, \mathbf{s}_g)$, where $\mathbf{z} = (z_{ndf}, z_{nsc}, z_{pro})$ is the vector
140 of concentrations of the polymer components (neutral detergent fiber, non-structural
141 carbohydrates and proteins; g/L), $\mathbf{s} = (s_{su}, s_{aa}, s_{ac}, s_{bu}, s_{pr}, s_{in}, s_{ic}, s_{H_2}, s_{CH_4}, s_{br})$ is the
142 vector of concentrations of the soluble components (sugars, amino acids, acetate, butyrate,
143 propionate, inorganic nitrogen, inorganic carbon, hydrogen, CH₄ and bromoform; mol/L), $\mathbf{x} =$
144 $(x_{su}, x_{aa}, x_{H_2})$ is the vector of concentrations of the microbial functional groups (sugars
145 utilizers, amino acids utilizers and hydrogen utilizers; mol/L), $\mathbf{s}_g = (s_{g,CO_2}, s_{g,H_2}, s_{g,CH_4})$ is the
146 vector of concentrations in gas phase (carbon dioxide, hydrogen and CH₄; mol/L). The polymer
147 components include an input flux in their equation and all the components are associated with
148 an output flux in liquid or gas phase. The input flux (g/(Lh)) of polymer components is
149 described as

$$150 F_{i,in} = \frac{w_i \cdot DMI}{V_l} \quad (2)$$

151 where w_i is the fraction of polymer component i in the diet of the animal, DMI is the DM
152 intake (g/h) with a total DM of 11.25 g split in two feed distributions along the day with the
153 first distribution accounts for 70% of the total DM, and V_l the volume in liquid phase of the
154 rumen (L).

155 The output flux in liquid phase (g/(Lh) for polymer components and mol/(Lh) for soluble and
156 microbial functional groups components) is described as

157
$$F_{i,out,l} = D \cdot z_i, \text{ for polymer components} \quad (3)$$

158
$$F_{i,out,l} = D \cdot s_i, \text{ for soluble components} \quad (4)$$

159
$$F_{i,out,l} = D \cdot x_i, \text{ for microbial functional groups} \quad (5)$$

160 where D is the dilution rate ($D = 0.035 \text{ h}^{-1}$, Bayat et al., 2011), z_i is the concentration of
 161 polymer component i , s_i is the concentration of soluble component i and x_i is the
 162 concentration of microbial functional group i .

163 The output flux in gas phase (mol/(Lh)) is described as

164
$$F_{i,out,g} = \frac{q_g \cdot s_{g,i}}{V_g} \quad (6)$$

165 where $q_g = \frac{R \cdot T \cdot V_1 \cdot (\rho_{T,H_2} + \rho_{T,CO_2} + \rho_{T,CH_4})}{P - p_{H_2O}}$ is the output flow of gas phase (L/h) wit R the ideal
 166 gas constant (barL/(molK)), T the temperature of the rumen (K), ρ_{T,H_2} , ρ_{T,CO_2} and ρ_{T,CH_4} the
 167 liquid-gas transfer phenomena rates of hydrogen, carbon dioxide and CH_4 (mol/(Lh)),
 168 respectively, P the total pressure (bars) and p_{H_2O} the partial pressure of water vapor (bar).
 169 $s_{g,i}$ is the concentration of component i in gas phase (mol/L) and V_g is the volume in gas
 170 phase of the rumen (L).

171 Model equations are derived from mass balance equations described below.

172 *For polymer components*

173
$$\frac{dz_{ndf}}{dt} = F_{ndf,in} - \rho_{ndf} - F_{ndf,out,l} \quad (7)$$

174
$$\frac{dz_{nsc}}{dt} = F_{nsc,in} - \rho_{nsc} + (f_{ch,x} \cdot w_{mb}) \cdot (\rho_{x_{su}} + \rho_{x_{aa}} + \rho_{x_{H_2}}) - F_{nsc,out,l} \quad (8)$$

175
$$\frac{dz_{pro}}{dt} = F_{pro,in} - \rho_{pro} + (f_{pro,x} \cdot w_{mb}) \cdot (\rho_{x_{su}} + \rho_{x_{aa}} + \rho_{x_{H_2}}) - F_{pro,out,l} \quad (9)$$

176 where $F_{ndf,in}$, $F_{nsc,in}$ and $F_{pro,in}$ are the input fluxes of neutral detergent fiber, non-structural
 177 carbohydrates and proteins (g/(Lh)), respectively. ρ_{ndf} , ρ_{nsc} and ρ_{pro} are the hydrolysis rate
 178 functions of polymer components (g/(Lh)), indicating the kinetic of hydrolysis of polymer
 179 components. These functions are described as

180
$$\rho_i = k_{hyd,i} \cdot z_i \quad (10)$$

181 With $k_{hyd,i}$ the hydrolysis rate constant (h^{-1}) and z_i the concentration of polymer component
 182 i (g/L). $F_{ndf,out}$, $F_{nsc,out}$ and $F_{pro,out}$ are the output fluxes of polymer components (g/(Lh)). The
 183 middle part of equations (8) and (9) represents the recycling of dead microbial cells where
 184 $f_{ch,x}$, $f_{pro,x}$ are the fractions of carbohydrates and proteins of the biomass, w_{mb} is the
 185 molecular weight of microbial cells (g/mol) and $\rho_{x_{su}} = k_d \cdot x_{su}$, $\rho_{x_{aa}} = k_d \cdot x_{aa}$, $\rho_{x_{H_2}} =$
 186 $k_d \cdot x_{H_2}$ are the cell death rate of sugars utilizers, amino acids utilizers and hydrogen utilizers
 187 (mol/(Lh)) with k_d the rate of dead of microbial cells (h^{-1}).

188 *For soluble components*

189
$$\frac{ds_{su}}{dt} = \frac{\rho_{ndf}}{w_{su}} + \frac{\rho_{nsc}}{w_{su}} - \rho_{su} - F_{su,out,l} \quad (11)$$

190
$$\frac{ds_{aa}}{dt} = \frac{\rho_{pro}}{w_{aa}} - \rho_{aa} - F_{aa,out,l} \quad (12)$$

$$191 \quad \frac{ds_{H_2}}{dt} = Y_{H_2,su} \cdot \rho_{su} + Y_{H_2,aa} \cdot \rho_{aa} - \rho_{H_2} - \rho_{T,H_2} - F_{H_2,out,l} \quad (13)$$

$$192 \quad \frac{ds_{ac}}{dt} = Y_{ac,su} \cdot \rho_{su} + Y_{ac,aa} \cdot \rho_{aa} - F_{ac,out,l} \quad (14)$$

$$193 \quad \frac{ds_{bu}}{dt} = Y_{bu,su} \cdot \rho_{su} + Y_{bu,aa} \cdot \rho_{aa} - F_{bu,out,l} \quad (15)$$

$$194 \quad \frac{ds_{pr}}{dt} = Y_{pr,su} \cdot \rho_{su} + Y_{pr,aa} \cdot \rho_{aa} - F_{pr,out,l} \quad (16)$$

$$195 \quad \frac{ds_{IN}}{dt} = Y_{IN,su} \cdot \rho_{su} + Y_{IN,aa} \cdot \rho_{aa} + Y_{IN,H_2} \cdot \rho_{H_2} - F_{IN,out,l} \quad (17)$$

$$196 \quad \frac{ds_{IC}}{dt} = Y_{IC,su} \cdot \rho_{su} + Y_{IC,aa} \cdot \rho_{aa} + Y_{IC,H_2} \cdot \rho_{H_2} - \rho_{T,CO_2} - F_{IC,out,l} \quad (18)$$

$$197 \quad \frac{ds_{CH_4}}{dt} = Y_{CH_4,H_2} \cdot \rho_{H_2} - \rho_{T,CH_4} - F_{CH_4,out,l} \quad (19)$$

198 Let us detail how the amino acids are produced and used by the biological pathways in the
 199 fermentation process. Equation (12) indicates that amino acids are produced (positive sign in
 200 the equation) from the degradation of proteins, occurring with the kinetic rate ρ_{pro} (g/L h),
 201 which is divided by the molecular weight of the amino acids w_{aa} (g/mol). Moreover, amino
 202 acids are utilized (negative sign in the equation) by the biological pathways during the
 203 fermentation with the kinetic rate ρ_{aa} (mol/Lh). The kinetic rate ρ_{aa} is a function indicating
 204 the kinetic of utilization of amino acids during the fermentation and is described as

$$205 \quad \rho_{aa} = \frac{k_{m,aa} \cdot s_{aa} \cdot x_{aa}}{K_{S,aa} + s_{aa}} \quad (20)$$

206 With $k_{m,aa}$ the maximum specific utilization rate constant of amino acids (mol substrate/(mol
 207 biomass h)), s_{aa} the concentration of amino acids (mol/L), x_{aa} the concentration of amino
 208 acids-utilizing microbes (mol/L) and $K_{S,aa}$ the Monod affinity constant associated with the
 209 utilization of amino acids (mol/L). $F_{aa,out}$ is the output flux of amino acids concentration
 210 (mol/(Lh)). Then, further in the fermentation, amino acids are utilized by the specific microbial
 211 functional group x_{aa} and contributed to the production of hydrogen (Equation 13), VFA
 212 (Equations 14, 15, 16), inorganic nitrogen (Equation 17) and inorganic carbon (Equation 18)
 213 with a stoichiometry represented by the yield factors $Y_{H_2,aa}$, $Y_{ac,aa}$, $Y_{bu,aa}$, $Y_{pr,aa}$, $Y_{IN,aa}$ and
 214 $Y_{IC,aa}$, respectively. These components are also produced from glucose metabolism. In the last
 215 step of the biochemical conversion cascade, inorganic nitrogen and inorganic carbon are
 216 utilized during the reaction of hydrogen utilization in liquid phase with the kinetic rate
 217 function ρ_{H_2} (mol/L h), described similarly as Equation (20). An additional term (I_{br}) is included
 218 to represent the inhibition effect of bromoform on the hydrogen utilizers (methanogens) as
 219 detailed later on. Hydrogen in liquid phase is also associated with a transfer phenomenon with
 220 hydrogen in gas phase given by the rate ρ_{T,H_2} (mol/(Lh)). This liquid-gas transfer phenomenon
 221 also concerns carbon dioxide with the rate ρ_{T,CO_2} (mol/(Lh)) and CH₄ (Equation 19) with the
 222 rate ρ_{T,CH_4} (mol/(Lh)). The general equation of the liquid-gas transfer rate is described as

$$223 \quad \rho_{T,i} = k_L a_i (s_i - K_{H,i} \cdot p_{g,i}) \quad (21)$$

224 With $k_{L,i}$ the mass transfer coefficient (h^{-1}), s_i the concentration (mol/L), $K_{H,i}$ the Henry's law
 225 coefficient (M/bar) and $p_{g,i}$ the partial pressure (bars) of soluble component i .

226 Finally, CH_4 in liquid phase is produced using hydrogen in liquid phase with the stoichiometry
 227 $Y_{\text{CH}_4, \text{H}_2}$.

228 *For microbial functional groups*

$$229 \quad \frac{dx_{\text{su}}}{dt} = Y_{\text{su}} \cdot \rho_{\text{su}} - \rho_{x_{\text{su}}} - F_{x_{\text{su}}, \text{out}, \text{l}} \quad (22)$$

$$230 \quad \frac{dx_{\text{aa}}}{dt} = Y_{\text{aa}} \cdot \rho_{\text{aa}} - \rho_{x_{\text{aa}}} - F_{x_{\text{aa}}, \text{out}, \text{l}} \quad (23)$$

$$231 \quad \frac{dx_{\text{H}_2}}{dt} = Y_{\text{H}_2} \cdot \rho_{\text{H}_2} - \rho_{x_{\text{H}_2}} - F_{x_{\text{H}_2}, \text{out}, \text{l}} \quad (24)$$

232 Microbial functional groups of glucose utilizers (Equation 22), amino acid utilizers (Equation
 233 23) and hydrogen utilizers (Equation 24) are produced from their respective substrates with
 234 the yield factors Y_{su} , Y_{aa} and Y_{H_2} , respectively.

235 *For the gas phase*

$$236 \quad \frac{ds_{\text{g}, \text{CO}_2}}{dt} = V_1 \cdot \frac{\rho_{\text{T}, \text{CO}_2}}{V_{\text{g}}} - F_{\text{CO}_2, \text{out}, \text{g}} \quad (25)$$

$$237 \quad \frac{ds_{\text{g}, \text{H}_2}}{dt} = V_1 \cdot \frac{\rho_{\text{T}, \text{H}_2}}{V_{\text{g}}} - F_{\text{H}_2, \text{out}, \text{g}} \quad (26)$$

$$238 \quad \frac{ds_{\text{g}, \text{CH}_4}}{dt} = V_1 \cdot \frac{\rho_{\text{T}, \text{CH}_4}}{V_{\text{g}}} - F_{\text{CH}_4, \text{out}, \text{g}} \quad (27)$$

239 The dynamics of carbon dioxide (Equation 25), hydrogen (Equation 26) and CH_4 (Equation
 240 27) in gas phase are driven by the liquid-gas transfer phenomena given by the rates $\rho_{\text{T}, \text{CO}_2}$,
 241 $\rho_{\text{T}, \text{H}_2}$ and $\rho_{\text{T}, \text{CH}_4}$ ($\text{mol}/(\text{Lh})$), respectively.

242 Model parameters were either set with values extracted from the literature (Batstone et al.,
 243 2002; Serment et al., 2016), set with values reported from *in vitro* study providing the
 244 experimental data (Chagas et al., 2019) or estimated using the maximum likelihood
 245 estimator as reported in Muñoz-Tamayo et al. (2021). In the present study, initial conditions
 246 of state variables were determined by running the model for 50 days without AT supply
 247 (control condition). The idea was to reach a quasi-steady state of the state variables. Values
 248 corresponding to the last time step simulated were selected as initial conditions of the
 249 model for the further analysis explained below.

250 **2.1.3. Integration of the macroalgae *Asparagosis*** 251 ***taxiformis***

252 The integration of bromoform contained in AT conducted to the incorporation of the 19th state
 253 variable representing the dynamic of bromoform concentration.

$$254 \quad \frac{ds_{\text{br}}}{dt} = F_{\text{br}, \text{in}} - k_{\text{br}} \cdot s_{\text{br}} - F_{\text{br}, \text{out}} \quad (28)$$

255 Where $F_{\text{br}, \text{in}} = \frac{w_{\text{br}} \cdot \text{DMI}}{V_1}$ is the input flux of bromoform concentration ($\text{g}/(\text{Lh})$) with w_{br} the
 256 fraction of bromoform in the diet of the animal. k_{br} corresponds to the kinetic rate of

257 bromoform utilization (h^{-1}) and $F_{\text{br,out}} = D \cdot s_{\text{br}}$ is the output flux of bromoform
 258 concentration ($\text{g}/(\text{Lh})$). The value of k_{br} was obtained from data reported in Romero et al.
 259 (2023b).

260 The direct effect of bromoform on the CH_4 production is represented through the factor I_{br}
 261 (Equation 29) impacting the kinetic rate function of hydrogen utilization (ρ_{H_2}). This factor is a
 262 function of the bromoform concentration and is modeled by a sigmoid shape. Whereas the
 263 indirect effect of bromoform on the flux allocation towards VFA production is represented
 264 through the flux allocation parameters λ , describing the 3 reactions driving flux allocation
 265 from glucose utilization to VFA production. λ_1 , λ_2 and λ_3 indicates the molar fraction of
 266 glucose utilized to produce acetate, to produce propionate and to produce butyrate,
 267 respectively. They follow $\lambda_1 + \lambda_2 + \lambda_3 = 1$. λ_1 (Equation 30) and λ_2 (Equation 31) are
 268 represented by affine functions described below.

$$269 \quad I_{\text{br}} = 1 - \frac{1}{1 + \exp(-p_1 \cdot (s_{\text{br}} + p_2))} \quad (29)$$

270 With s_{br} the bromoform concentration (g/L) and p_1, p_2 the parameters of sigmoid function.

$$271 \quad \lambda_1 = p_3 - p_4 \cdot p_{\text{H}_2} \quad (30)$$

272 With p_{H_2} the hydrogen partial pressure (bars) and p_3, p_4 the parameters of affine function.

$$273 \quad \lambda_2 = p_5 + p_6 \cdot p_{\text{H}_2} \quad (31)$$

274 With p_{H_2} the hydrogen partial pressure (bars) and p_5, p_6 the parameters of affine function.

275 These factors are displayed in Figure 4.

276

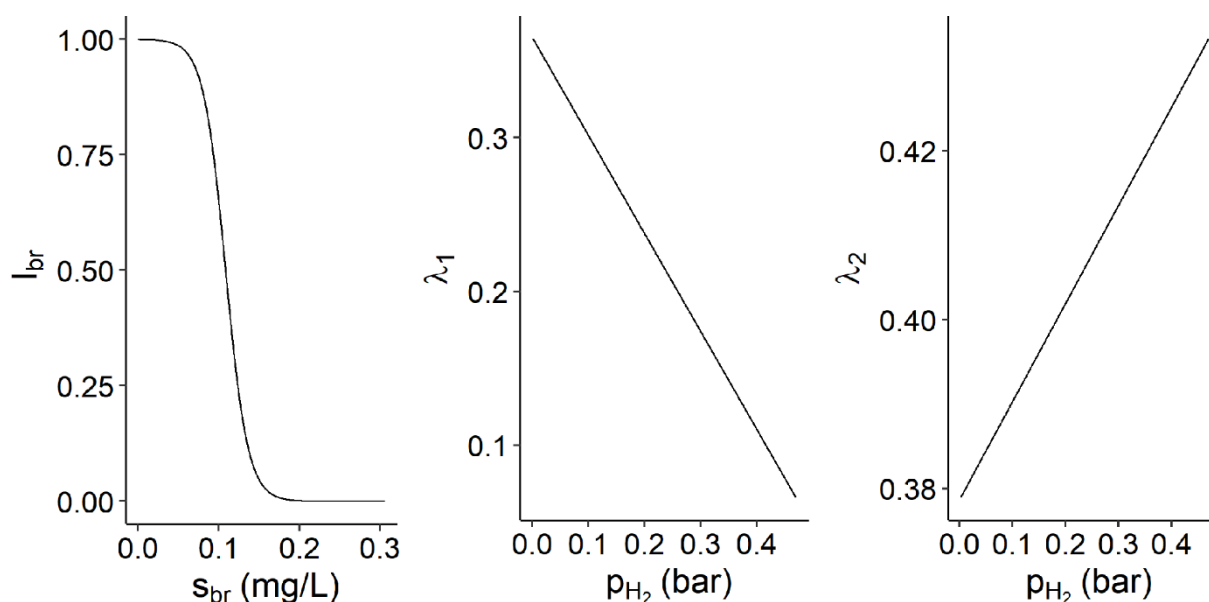


Figure 4. Representation of the direct effect of *Asparagosis taxiformis* on the methane production (I_{br}) against the bromoform concentration (s_{br} , mg/L), and of the indirect effect of *Asparagosis taxiformis*, through the hydrogen accumulation, on the flux allocation towards acetate production (λ_1) and propionate production (λ_2) against the hydrogen partial pressure (p_{H_2}).

277

278 It should be noted that the model version of Muñoz-Tamayo et al. (2021) includes an inhibition
 279 factor of glucose utilization by hydrogen (I_{H_2}). This factor was incorporated to account for the
 280 reduced production of VFA under AT supply observed in the experiments of Chagas et al.
 281 (2019). However, in the present study, we decided not to include this term. Some studies have
 282 shown that high doses of AT decrease total VFA both *in vitro* (Chagas et al., 2019; Kinley et al.,
 283 2016; Machado et al., 2016; Terry et al., 2023) and *in vivo* (Li et al., 2016; Stefenoni et al.,
 284 2021). However, in other studies the total VFA was unaffected by AT supplementation under
 285 *in vitro* (Romero et al., 2023b; Roque et al., 2019) and *in vivo* (Kinley et al., 2020) conditions.
 286 These discrepancies might be due to the variability of physical processing of the macroalgae
 287 (e.g., drying, storage). The incorporation of the hydrogen inhibition factor was indeed
 288 challenged by Henk Van Lingen in the evaluation of the model in Muñoz-Tamayo et al., (2021)
 289 (Tedeschi, 2021). Accordingly, we acknowledge that this aspect requires further studies, and
 290 it is not then included in the present work. We then run again the calibration of the model
 291 without the I_{H_2} factor under batch conditions using the experimental data from Chagas et al.
 292 (2019) to estimate the parameters from equations (28-30). In the process, with the aim of
 293 model simplification, we set the allocation factors λ_1 , λ_2 as linear functions of p_{H_2} . The
 294 updated version of the model under batch conditions is available at Muñoz-Tamayo (2020).
 295

296 **Table 1.** Stoichiometry matrix of biochemical reactions occurring during the rumen
 297 fermentation.

Component → i	1	2	3	4	5	6	7	8	Kinetic rate
j Microbial process ↓	Z_{ndf}	Z_{nsc}	Z_{pro}	S_{su}	S_{aa}	S_{H_2}	S_{ac}	S_{bu}	
1 Hydrolysis of NDF	-1			$1/w_{su}$					ρ_{ndf}
1 Hydrolysis of NSC		-1		$1/w_{su}$					ρ_{nsc}
2 Hydrolysis of proteins			-1		$1/w_{aa}$				ρ_{pro}
3 Utilization of glucose				-1		$Y_{H_2,su}$	$Y_{ac,su}$	$Y_{bu,su}$	ρ_{su}
4 Utilization of amino acids					-1	$Y_{H_2,aa}$	$Y_{ac,aa}$	$Y_{bu,aa}$	ρ_{aa}
5 Utilization of hydrogen						-1			ρ_{H_2}
6 Death of sugars utilizers		$f_{ch,x} \cdot W_{mb}$	$f_{pro,x} \cdot W_{mb}$						$\rho_{x_{su}}$
7 Death of amino acids utilizers		$f_{ch,x} \cdot W_{mb}$	$f_{pro,x} \cdot W_{mb}$						$\rho_{x_{aa}}$
8 Death of hydrogen utilizers		$f_{ch,x} \cdot W_{mb}$	$f_{pro,x} \cdot W_{mb}$						$\rho_{x_{H_2}}$
9 Inhibition of bromoform									

Component → i	9	10	11	12	13	14	15	16	Kinetic rate
j Microbial process ↓	S_{pr}	S_{IN}	S_{IC}	S_{CH_4}	x_{su}	x_{aa}	x_{H_2}	S_{br}	
1 Hydrolysis of NDF									ρ_{ndf}
1 Hydrolysis of NSC									ρ_{nsc}
2 Hydrolysis of proteins									ρ_{pro}
3 Utilization of glucose	$Y_{pr,su}$	$Y_{IN,su}$	$Y_{IC,su}$		Y_{su}				ρ_{su}
4 Utilization of amino acids	$Y_{pr,aa}$	$Y_{IN,aa}$	$Y_{IC,aa}$			Y_{aa}			ρ_{aa}
5 Utilization of hydrogen		Y_{IN,H_2}	Y_{IC,H_2}	Y_{CH_4,H_2}			Y_{H_2}		ρ_{H_2}
6 Death of sugars utilizers					-1				$\rho_{x_{su}}$
7 Death of amino acids utilizers						-1			$\rho_{x_{aa}}$
8 Death of hydrogen utilizers							-1		$\rho_{x_{H_2}}$
9 Inhibition of bromoform								$-k_{br}$	

298

299 **Table 2.** Model parameters

	Definition	Unit	Value	Reference
Rates				
μ_j	Growth rate of the microbial group j	mol j/(L h)	$Y_j \cdot \rho_j$	
ρ_j	Kinetic rate of microbial process j	Mol (or g) j/(L h)	$k_{m,j} \frac{S_j}{K_{s,j} + S_j} x_j$	
ρ_{x_j}	Death cell rate of microbes j	mol j/(L h)	$k_d \cdot x_j$	
$\rho_{T,j}$	Liquid-gas transfer rate of component j	mol j/(L h)	$k_{L,a} \cdot (S_j - K_{H,j} \cdot p_{gas,j})$	
Biochemical parameters				
λ_1	Molar fraction of the sugars utilized to produce acetate	mol/mol	$p_3 - p_4 \cdot p_{H_2}$	
λ_2	Molar fraction of the sugars utilized to produce acetate	mol/mol	$p_5 + p_6 \cdot p_{H_2}$	
λ_3	Molar fraction of the sugars utilized to produce acetate	mol/mol	$1 - (\lambda_1 + \lambda_2)$	
$\sigma_{ac,aa}$	Stoichiometry coefficient of acetate production from amino acids utilization	mol/mol	0.67	
$\sigma_{bu,aa}$	Stoichiometry coefficient of butyrate production from amino acids utilization	mol/mol	0.24	
$\sigma_{pr,aa}$	Stoichiometry coefficient of propionate production from amino acids utilization	mol/mol	0.062	
$\sigma_{H_2,aa}$	Stoichiometry coefficient of hydrogen production from amino acids utilization	mol/mol	0.82	
$\sigma_{IC,aa}$	Stoichiometry coefficient of inorganic carbon production from amino acids utilization	mol/mol	0.88	
f_{H_2}	Fraction of hydrogen utilized for product formation	mol/mol	$1 - 10 \cdot Y_{H_2}$	
f_{su}	Fraction of glucose utilized for product formation	mol/mol	$1 - \frac{5}{6} \cdot Y_{su}$	
$f_{ch,x}$	Mass fraction of carbohydrates in the microbial cells	g/g	0.20	
$f_{pro,x}$	Mass fraction of proteins in the microbial cells	g/g	0.55	
k_{br}	Kinetic rate constant of bromoform utilization	h ⁻¹	0.095	Romero et al., 2023b
k_d	Death cell rate constant	h ⁻¹	8.33e-04	
$k_{hyd,ndf}$	Hydrolysis rate constant of cell wall carbohydrates	h ⁻¹	0.024	
$k_{hyd,nsc}$	Hydrolysis rate constant of non-structural carbohydrates	h ⁻¹	0.06	
$k_{hyd,pro}$	Hydrolysis rate constant of proteins	h ⁻¹	0.09	
$k_{m,aa}$	Maximum specific utilization rate constant of amino acids	mol/(mol h)	2.00	
k_{m,H_2}	Maximum specific utilization rate constant of hydrogen	mol/(mol h)	16	
$k_{m,su}$	Maximum specific utilization rate constant of glucose	mol/(mol h)	1.00	
$K_{s,aa}$	Monod constant associated with the utilization of amino acids	mol/L	6.40e-03	
K_{s,H_2}	Monod constant associated with the utilization of hydrogen	mol/L	5.84e-06	
$K_{s,su}$	Monod constant associated with the utilization of glucose	mol/L	9.00e-03	

$K_{s,IN}$	Nitrogen limitation constant	mol/L	2.0e-04	
Y_{aa}	Microbial biomass yield factor of amino acids utilizers	mol/mol	0.31	
Y_{H_2}	Microbial biomass yield factor of hydrogen utilizers	mol/mol	0.006	
Y_{su}	Microbial biomass yield factor of glucose utilizers	mol/mol	0.16	
$Y_{ac,su}$	Yield factor of the acetate during utilization of glucose	mol/mol	$f_{su} \cdot (2 \cdot \lambda_1 + \frac{2}{3} \cdot \lambda_2)$	
$Y_{bu,su}$	Yield factor of the butyrate during utilization of glucose	mol/mol	$f_{su} \cdot (\lambda_3)$	
$Y_{pr,su}$	Yield factor of the propionate during utilization of glucose	mol/mol	$f_{su} \cdot (\frac{4}{3} \cdot \lambda_2)$	
$Y_{H_2,su}$	Yield factor of the hydrogen during utilization of glucose	mol/mol	$f_{su} \cdot (4 \cdot \lambda_1 + 2 \cdot \lambda_3)$	
$Y_{IN,su}$	Yield factor of the inorganic nitrogen during utilization of glucose	mol/mol	$-Y_{su}$	
$Y_{IC,su}$	Yield factor of the inorganic carbon during utilization of glucose	mol/mol	$f_{su} \cdot (2 \cdot \lambda_1 + \frac{2}{3} \cdot \lambda_2 + 2 \cdot \lambda_3)$	
Y_{CH_4,H_2}	Yield factor of the methane during utilization of hydrogen	mol/mol	$f_{H_2} \cdot (\frac{1}{4})$	
Y_{IC,H_2}	Yield factor of the inorganic carbon during utilization of hydrogen	mol/mol	$-(\frac{1}{4} \cdot f_{H_2} + (\frac{5}{10}) \cdot (1 - f_{H_2}))$	
Y_{IN,H_2}	Yield factor of the inorganic nitrogen during utilization of hydrogen	mol/mol	$-Y_{H_2}$	
$Y_{i,aa}$	Yield factor of the component i during utilization of amino acids	mol/mol	$(1 - Y_{aa}) \cdot \sigma_{i,aa}$	
$Y_{IN,aa}$	Yield factor of the component inorganic nitrogen during utilization of amino acids	mol/mol	$N_{aa} - Y_{aa} \cdot N_{mb}$	
Physicochemical parameters				
K_{a,CO_2}	Equilibrium constant of bicarbonate		5.13e-07	Batstone et al., 2002
K_{a,NH_4}	Equilibrium constant of ammonium		1.44e-09	Batstone et al., 2002
$K_{a,VFA}$	Equilibrium constant of VFA		1.74e-05	Batstone et al., 2002
K_w	Equilibrium coefficient of water		2.75e-14	Batstone et al., 2002
$k_L a$	Liquid-gas transfer constant	h^{-1}	8.33	
K_{H,CO_2}	Henry's law coefficient of carbon dioxide	M/bar	2.46e-02	Batstone et al., 2002
K_{H,CH_4}	Henry's law coefficient of methane	M/bar	1.10e-03	Batstone et al., 2002
K_{H,H_2}	Henry's law coefficient of hydrogen	M/bar	7.23e-04	Batstone et al., 2002
P	Pressure	bars	1.01325	Serment et al., 2016
T	Temperature	K	312.15	Serment et al., 2016
w_{aa}	Molecular weight of average amino acid	g/mol	134	Feedpedia
w_{ac}	Molecular weight of acetate	g/mol	60.05	Wikipedia
w_{bu}	Molecular weight of butyrate	g/mol	88.10	Wikipedia
w_{mb}	Molecular weight of microbial cells	g/mol	113	Batstone et al., 2002
w_{pr}	Molecular weight of propionate	g/mol	74.1	Wikipedia
w_{su}	Molecular weight of glucose	g/mol	180.16	Wikipedia

V_g	Volume of the gas phase	L	0.06	Belanche et al., 2017
V_l	Volume of the liquid phase	L	0.74	Belanche et al., 2017
Parameters of factors modelling the effect of bromoform on rumen fermentation				
p_1	Parameter of the factor I_{br} modelling the direct effect of bromoform on the CH ₄ production		72551	
p_2	Parameter of the factor I_{br} modelling the direct effect of bromoform on the CH ₄ production		-1.0837e-04	
p_3	Intercept of λ_1		0.3655	
p_4	Slope of λ_1		0.6371	
p_5	Intercept of λ_2		0.3787	
p_6	Slope of λ_2		0.1160	

300

301 2.2. Sensitivity analysis

302 We implemented two SA methods for quantifying the contribution of 16 IPs to the variability
 303 of 4 state variables of the mechanistic model described in the previous section. These 2
 304 methods use a strong theoretical framework and provide easy-to-interpret sensitivity indices
 305 (SI). Moreover, the SI were computed over time allowing to study the dynamic of IP sensitivity
 306 during the fermentation. Thus, Shapley effects (Owen, 2014) and full and independent Sobol
 307 indices (Mara et al., 2015) were computed for quantifying the individual, interaction and
 308 dependence/correlation effects of an IP to the variability of an output. Although the model
 309 studied here provides no correlated or dependent IPs, these 2 methods were used to
 310 introduce a new SA method in the animal science field.

311 This work was done with the support of MESO@LR-Platform at the University of Montpellier,
 312 which was used to run the algorithms computing Shapley effects and Sobol indices. They were
 313 run using one node, 28 cores and 125 GB of RAM of memory.

314 2.2.1. Input parameters and output variables studied

315 State variables of the model considered as output variables of the SA were the rate of CH₄
 316 production (in gas phase) ($q_{CH_4,g,out}$, mol/h) and VFA (acetate (s_{ac}), butyrate (s_{bu}) and
 317 propionate (s_{pr})) concentrations (mol/L). The model was runned for 4 days, similarly to the
 318 RUSITEC of Roque et al., (2019), and the SA was performed on the last day of simulation, from
 319 72 to 96h with a time step of 1h.

320 Components constituting the model represent different factors associated to microbial
 321 pathways involved in *in vitro* rumen fermentation. These factors include polymer hydrolysis
 322 and microbial growth. The sensibility of hydrolysis rate constants associated with the 3
 323 polymer components ($k_{hyd,ndf}$, $k_{hyd,nsc}$ and $k_{hyd,pro}$, h⁻¹) was studied for quantifying the
 324 impact of feed polymer hydrolysis on output variables of interest during the fermentation. In
 325 addition, the sensibility of maximum specific utilization rate constants ($k_{m,su}$, $k_{m,aa}$ and k_{m,H_2} ,
 326 mol substrate/(mol biomass h)) and Monod constants ($K_{S,su}$, $K_{S,aa}$ and K_{S,H_2} , mol/L)

327 associated with the 3 microbial groups was studied for quantifying the impact of microbial
328 growth on output variables of interest during the fermentation.

329 In addition to the IPs quantifying the impact of polymer components and microbial functional
330 groups, IPs related to the effect of bromoform on the fermentation were considered. The
331 kinetic rate constant of bromoform utilization (k_{br} , h^{-1}), quantifying the consumption of anti-
332 methanogenic compounds, was added to the SA. Moreover, the parameters of sigmoid and
333 affine functions associated with the factor representing the impact of bromoform on
334 methanogens (I_{br} associated with parameters p_1 and p_2) and with the flux allocation from
335 glucose utilization to VFA production (λ_1 associated with parameters p_3 and p_4 , and λ_2
336 associated with parameters p_5 and p_6) were added to the SA. Therefore, in total, 16 IPs were
337 considered.

338 The first step in SA was to set the variability space of IPs. To perform that, information about
339 the variability of each IP was required. This information was available from 2 sources: data
340 and expert knowledge (Table 3). Based on the low number of data available for each IP,
341 uniform distributions were selected for quantifying hydrolysis rate constants, maximum
342 specific utilization rate constants and Monod constants variability. Lower and upper bounds
343 of uniform distributions were set by selecting the minimum and maximum values among all
344 the references. Furthermore, the parameters associated with the effect of bromoform on the
345 fermentation were not biological parameters and no data were available for modeling their
346 variability. Therefore, a uniform distribution varying of $\pm 10\%$ the baseline model parameter
347 value was used for parameters p_1 to p_6 .

348
349 **Table 3.** Variation range (minimum (min) and maximum (max)) and sources/references of
350 uniform distributions used for exploring the variability of input parameters studied in the
351 sensitivity analysis.

Parameter	Min	Max	References
$k_{hyd,ndf}$	0.01	0.33	Chapoutot et al., 2010; Muñoz-Tamayo et al., 2016; van Lingen et al., 2019
$k_{hyd,nsc}$	0.06	0.22	Muñoz-Tamayo et al., 2016; van Lingen et al., 2019
$k_{hyd,pro}$	0.05	0.25	Muñoz-Tamayo et al., 2016; van Lingen et al., 2019
$k_{m,su}$	0.94	4.33	Batstone et al., 2002; Muñoz-Tamayo et al., 2021, 2016
$K_{S,su}$	1e-04	9e-03	Batstone et al., 2002; Muñoz-Tamayo et al., 2021, 2016
$k_{m,aa}$	1	5	Batstone et al., 2002; Muñoz-Tamayo et al., 2021, 2016
$K_{S,aa}$	3e-04	8e-03	Batstone et al., 2002; Muñoz-Tamayo et al., 2021, 2016
k_{m,H_2}	12	25	Batstone et al., 2002; Muñoz-Tamayo et al., 2021, 2016
K_{S,H_2}	1e-07	1e-05	Batstone et al., 2002; Muñoz-Tamayo et al., 2021, 2016
k_{br}	8.55e-02	1.04e-01	
p_1	6.52e+04	7.98e+04	
p_2	-1.19e-04	-9.75e-05	
p_3	0.33	0.40	
p_4	0.57	0.70	
p_5	0.34	0.42	

p_6 0.10 0.13

352

353 2.2.2. System characteristics, intake and dietary scenarios

354 The consideration of feed intake in the model studied allows to simulate dietary scenarios.
 355 The dietary scenarios studied in this work were set using data from an *in vitro* study assessing
 356 several dietary CH₄ mitigation strategies, including AT, on the fermentation (Chagas et al.,
 357 2019). This experiment tested the impact on CH₄ production of several doses of AT from 0 to
 358 1% DM (containing 6.84 mg/g dry weight of bromoform) in the diet. The diet was composed
 359 of 38.7% DM of neutral detergent fiber, 39.7% DM of non-structural carbohydrates and 16%
 360 DM of crude proteins. We analyzed three simulation scenarios: A control treatment with 0%
 361 of AT, a low treatment with 0.25% of AT and a high treatment with 0.50% of AT (Figure 5).
 362

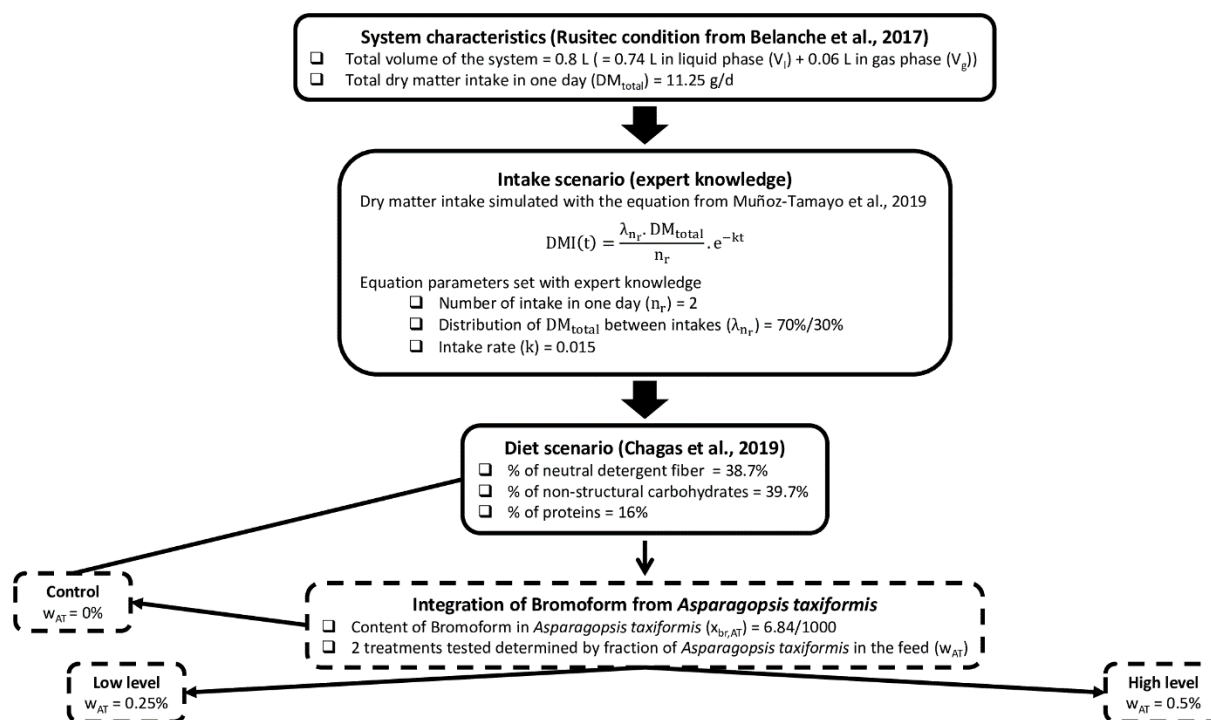


Figure 5. Summary of system characteristics, intake scenario and diet scenario simulated with the mechanistic model.

363

364 The initial condition of bromoform concentration was set to zero for all the 3 treatments.

365

366 2.2.3. Shapley effects

367 2.2.3.1. Definition

368 The first method implemented was the Shapley effects, which come from the field of
 369 cooperative game theory (Shapley, 1953). The Shapley effect of an IP X_i (Sh_i) measures the

370 part of variability of the output variable caused by the variability of X_i , and allocate to X_i a fair
371 value regarding its individual contribution, its contribution due to interactions with other IPs
372 and its contribution due to dependence/correlation with other IPs (Owen, 2014, Song et al.,
373 2016). It is described as

$$374 \quad Sh_i = \frac{1}{d} \sum_{u \subseteq -\{i\}} \binom{d-1}{|u|}^{-1} \left(\sum_{v \subseteq u+i} \text{Var}(E[Y|X_v]) - \sum_{v \subseteq u} \text{Var}(E[Y|X_v]) \right) \quad (32)$$

375 where d is the number of IPs, $u \subseteq \{1, \dots, d\}$ is a subset of IPs, Y is the output variable and X is
376 an IP.

377 **2.2.3.2. Interpretation**

378 The Shapley effects are condensed and easy-to-interpret. Their sum is equal to 1, allowing us
379 to interpret them as the percentage of contribution of the IPs to output variability.
380 Nevertheless, the distinction of individual, interaction and dependence/correlation effects are
381 not possible. Each IP is associated with one value, integrating the 3 effects.

382 **2.2.3.3. Numerical computation**

383 Several methods are available for estimating the Shapley effects. In our study, the random
384 permutation method was used (Song et al., 2016). This method provides a consistent
385 estimation of the Shapley effects adapted in the case of numerous IPs (Iooss and Prieur, 2019).
386 It is based on an alternative definition of the Shapley effects, expressing it in terms of all the
387 possible IPs permutations (Castro et al., 2009). The cost of this method is $N_v + m(d-1)N_oN_i$
388 with N_v the sample size for estimating the output variance, m the number of permutations
389 randomly sampled from the space of all the possible IP permutations, d the number of IPs
390 considered, N_o the sample size for estimating the expectation and N_i the sample size for
391 estimating the conditional variance. N_o and N_i were set at 1 and 3, respectively, as
392 recommended in Song et al. (2016). In addition, $N_v = 1e04$ and $m = 1e04$ were considered,
393 conducting to 460000 model evaluations. Estimation of the Shapley effects was performed
394 using the R package "sensitivity" (Iooss et al., 2023).

395 **2.2.4. Full and independent Sobol indices**

396 **2.2.4.1. Definition**

397 Sobol indices (Sobol, 1993) are commonly used when performing SA. The first-order Sobol
398 indice (S_i) of an IP X_i quantifies the individual contribution of X_i to output variability, based
399 on the variance decomposition such as

$$400 \quad S_i = \frac{\text{Var}(E[Y|X_i])}{\text{Var}(Y)} \quad (33)$$

401 where Y is the output variable and X_i is an IP. In addition, the total Sobol index (T_i) (Homma
402 and Saltelli, 1996) quantifies the contribution due to the interactions of X_i with other IPs such
403 as

$$404 \quad T_i = S_i + \sum_{j \neq i} S_{ij} + \sum_{j \neq i, k \neq i, j < k} S_{ijk} + \dots \quad (34)$$

405 where S_i is the first-order Sobol index of X_i , S_{ij} is the second-order Sobol index of X_i
406 quantifying the interactions between X_i and other IPs 2 by 2, S_{ijk} is the third-order Sobol index
407 of X_i quantifying the interactions between X_i and other IPs 3 by 3.

408 When dependence/correlation is present among the IPs, the variance decomposition is no
409 longer applicable. Then, S_i and T_i are no longer computable. In this case, Mara et al. (2015)
410 proposed Sobol indices allowing to quantify the contribution of an IP due to its
411 dependence/correlation with other IPs by computing 4 SI:

- 412 • the full first-order and total Sobol indices ($S_i^{\text{full}}, T_i^{\text{full}}$) of an IP X_i integrate the
413 dependence/correlation effects between X_i and other IPs;
- 414 • the independent first-order and total Sobol indices ($S_i^{\text{ind}}, T_i^{\text{ind}}$) of an IP X_i represent
415 the effects of X_i that are not due to its dependence/correlation with other IPs.

416 **2.2.4.2. Interpretation**

417 Sobol indices of Mara et al. (2015) are interpreted in 2 steps:

- 418 a. T_i^{full} and T_i^{ind} are compared for quantifying the contribution of X_i due to its
419 dependence/correlation effects.
 - 420 • The combination of a high T_i^{full} and a low T_i^{ind} indicates that X_i contributes to
421 output variability only via its dependence/correlation with other IPs;
 - 422 • a high T_i^{ind} indicates that X_i contributes to output variability via its own
423 variability and/or its interactions with other IPs;
 - 424 • a low T_i^{full} and T_i^{ind} indicates that X_i has no contribution on output variability
- 425 b. The second step of the interpretation is the comparison of S_i^{full} and T_i^{full} or S_i^{ind} and
426 T_i^{ind} , depending on whether X_i contributes to output variability via its
427 dependence/correlation with other IPs, for quantifying the contribution of X_i due to
428 its interaction effects:
 - 429 • $T_i - S_i \approx 0$ indicates that X_i contributes to output variability via its own
430 variability,
 - 431 • $T_i - S_i \gg 0$ indicates that X_i contributes to output variability via its
432 interactions with other IPs.

433 **2.2.4.3. Numerical computation**

434 For estimating the 4 indices, IPs were sampled using the Sobol sequences, which were
435 identified as providing a better stability for Sobol indices estimation (Blondiaux et al., 2022).
436 3000 simulations and 100 bootstrap replications using the Sobol (Sobol, 1993) and Saltelli

437 (Saltelli et al., 2008) estimators for computing first-order (S_i^{full} and S_i^{ind}) and total (T_i^{full} and
438 T_i^{ind}) indices, respectively, were conducted with the R package “sensobol” (Puy et al., 2022),
439 leading to 54000 model evaluations. Moreover, the estimation of conditional densities of the
440 IPs is required for modelling their dependence structure. This estimation was conducted using
441 a vine copula model.

442 In addition to the Shapley effects, the interpretation of S_i^{full} , T_i^{full} , S_i^{ind} and T_i^{ind} allows a
443 distinction of the individual, interaction and dependence/correlation effects. Therefore, in our
444 work, both methods were used in a complementary approach. First, the Shapley effects of the
445 16 IPs studied were computed for estimating their percentage of contribution, integrating the
446 3 effects, to the variability of output variables of interest. Second, the full and independent
447 Sobol indices were computed for identifying what is the main source of contribution among
448 these 3 effects.

449 **2.3. Uncertainty analysis**

450 SA provides a framework combining an IP sampling matrix, developed by randomly drawing
451 values from IP probability distributions, to simulations of our 4 outputs of interest. This *in silico*
452 framework was used for analyzing uncertainty associated with the simulations of CH₄, acetate,
453 butyrate and propionate concentrations (mol/L). Similarly to SA, uncertainty associated with
454 outputs of interest was studied dynamically by computing summary statistics (median,
455 standard deviation (SD), and quantiles 10 and 90%) and the coefficient of variation (CV) of the
456 output simulations at each time step.

457 **3. Results**

458 **3.1. Analysis of the simulations of the mechanistic model**

459 Figure 6 and Figure 7 display the dynamics of $q_{\text{CH}_4, \text{g, out}}$ and of VFA proportions, and
460 propionate to acetate ratio of the 3 dietary scenarios (control: 0% of AT, low treatment: 0.25%
461 of AT and high treatment: 0.50% of AT) for a 4 days simulation.

462

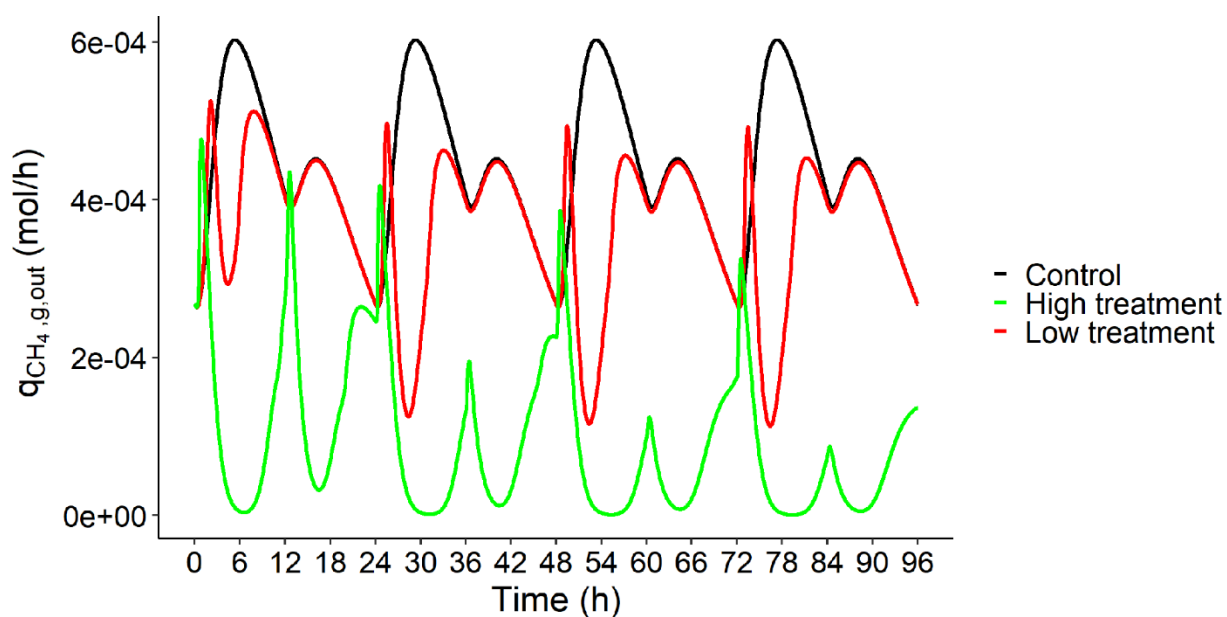


Figure 6. Rate of CH₄ production in gas phase ($q_{CH_4,g,out}$, mol/h) over time (h) of the 3 dietary scenarios (control: 0% of *Asparagopsis taxiformis*, low treatment: 0.25% of *Asparagopsis taxiformis* and high treatment: 0.50% of *Asparagopsis taxiformis*) for a 4 days simulation.

463

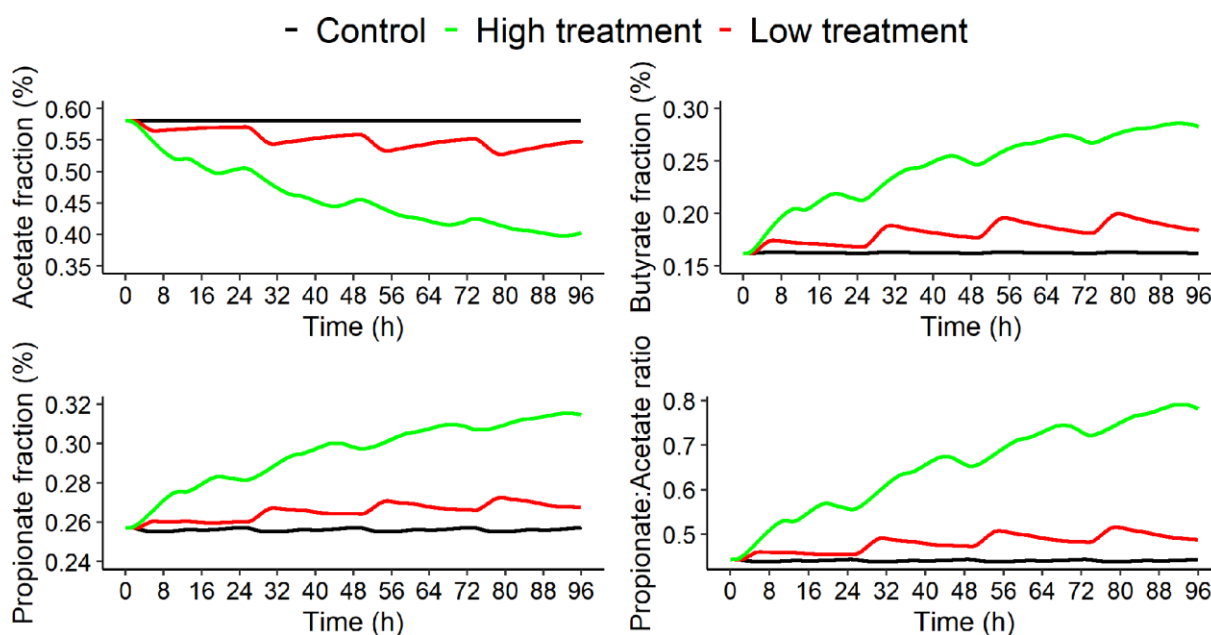


Figure 7. Acetate proportion (%), butyrate proportion (%), propionate proportion (%) and propionate to acetate ratio over time (h) of the 3 dietary scenarios (control: 0% of *Asparagopsis taxiformis*, low treatment: 0.25% of *Asparagopsis taxiformis* and high treatment: 0.50% of *Asparagopsis taxiformis*) for a 4 days simulation.

464

465 Increasing the dose of AT decreased $q_{CH_4,g,out}$ with, at the end of the 4 days of simulations, a
 466 CH₄ (g/d) reduction of 17% between control and low AT treatment and of 78% between
 467 control and high AT treatment. This reduction increased from one day to the next with
 468 computed reductions of 9%, 14%, 16% and 17% between control and low AT treatment, and

469 of 65%, 72%, 75% and 78% between control and high AT treatment, from day 1 to 4,
470 respectively.

471 The dynamic of VFA proportions showed that increasing AT dose in the diet decreased acetate
472 proportion of 5% and 31% at the end of the fermentation between control, and low and high
473 AT treatments, respectively. Whereas, butyrate and propionate proportions increased when
474 increasing AT dose in the diet, with increases at the end of the fermentation ($t = 96\text{h}$) of 13%
475 and 74% for butyrate proportion and of 4% and 22% for propionate proportion between
476 control, and low and high AT treatments, respectively.

477 Propionate to acetate ratio was also associated with an increase of 10% between control and
478 low AT treatment and of 76% between control and high AT treatment.

479 **3.2. Sensitivity analysis**

480 **3.2.1. Shapley effects**

481 Figure 8, Figure 9, Figure 10 and Figure 11 display the Shapley effects computed over time for
482 the 4th day of simulation (from 72 to 96h) of $q_{\text{CH}_4,\text{g},\text{out}}$ (mol/h), s_{ac} (mol/L), s_{bu} (mol/L) and
483 s_{pr} (mol/L), respectively, for the 3 dietary scenarios (control, low AT treatment and high AT
484 treatment) studied. Only the IP associated with a contribution higher than 10% for at least
485 one time step were displayed.

486 For some time steps, the computation led to negative indexes. In this case, the estimates were
487 set to 0. These issues mainly concerned $q_{\text{CH}_4,\text{g},\text{out}}$ of the 2 AT treatments and were either due
488 to the outliers in the variability explored in the simulations or to the lack of variability in the
489 simulations for some time steps. The computational time for one dietary scenario was of 24h
490 using the MESO@LR-Platform.

491 **3.2.1.1. Rate of methane production**

492 Figure 8 indicated that the microbial group of hydrogen utilizers, via the Monod affinity
493 constant K_{S,H_2} , contributed largely the most to the variability of $q_{\text{CH}_4,\text{g},\text{out}}$ over the
494 fermentation for control and low AT treatment, explaining more than 50% of $q_{\text{CH}_4,\text{g},\text{out}}$
495 variation over time for both scenarios. The influence of this IP was also important for high AT
496 treatment from 73 to 76h, from 87 to 89h and from 93 to 96h.

497

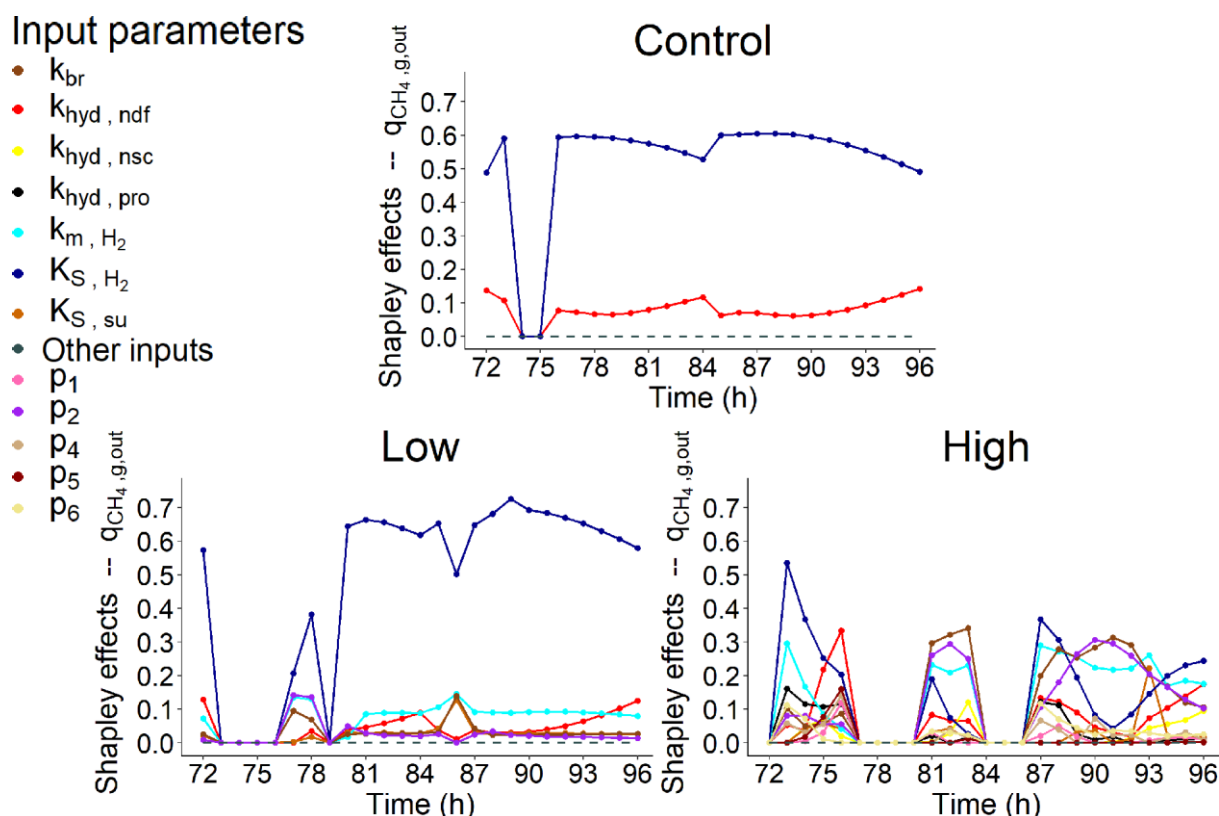


Figure 8. Shapley effects of the influential input parameters (*i.e.*, parameters with a contribution higher than 10% for at least one time step) over time (h) computed for the 4th day of simulation of the rate of CH₄ production in gas phase ($q_{CH_4, g, out}$, mol/h) for the 3 dietary scenarios (control: 0% of *Asparagopsis taxiformis*, low treatment: 0.25% of *Asparagopsis taxiformis* and high treatment: 0.50% of *Asparagopsis taxiformis*).

498
 499 The other influential IP for control was related to fiber degradation via the hydrolysis rate
 500 constant $k_{hyd, ndf}$, highlighting a contribution of c.a. 10% to $q_{CH_4, g, out}$ variability over time.
 501 This IP showed a low influence (c.a. 10%) for low and high AT treatments.
 502 Hydrogen utilizers microbial group also showed an influence via the maximum specific
 503 utilization rate constant k_{m, H_2} on $q_{CH_4, g, out}$ variation of low and high AT treatments. This
 504 influence was low (c.a. 10%) for low AT treatment over the fermentation and was of c.a. 20%
 505 or higher at $t = 73h$, from 81 to 83h and from 87 to 96h for high AT treatment.
 506 Moreover, for low and high AT treatments some IP associated with the factors modeling the
 507 effect of AT on the fermentation were highlighted. The IP p_2 , which is related to the sigmoid
 508 function modelling the direct inhibition effect of AT on methanogenesis, showed a
 509 contribution to $q_{CH_4, g, out}$ variability higher than 10% from 77 to 78h for low AT treatment and
 510 higher than 20% (most important contribution with the kinetic rate constant of bromoform
 511 utilization k_{br}) for high AT treatment. The IPs p_2 and k_{br} explained more than 50% of $q_{CH_4, g, out}$
 512 variability of high AT treatment at $t =$ from 81 to 83h and from 88 to 92h. Their influence
 513 decreased at the end of the fermentation but was still higher than 20%. When comparing both
 514 IPs, k_{br} showed a slightly higher influence (< 10%) than p_2 .

515 Finally, AT treatments highlighted the differences of the role of microbial pathways explaining
 516 the variation of $q_{\text{CH}_4,\text{g,out}}$ when increasing the dose of AT. The IPs $k_{\text{hyd},\text{nsc}}$, $k_{\text{hyd},\text{pro}}$, $K_{\text{S},\text{su}}$, p_1 ,
 517 p_4 , p_5 and p_6 showed a low but non-negligible influence (c.a. 10%) to $q_{\text{CH}_4,\text{g,out}}$ variability for
 518 high AT treatment and were not influential for control and low AT treatment, except $K_{\text{S},\text{su}}$
 519 which showed also a low influence (c.a. 10%) for low AT treatment.

520 3.2.1.2. Acetate concentration

521 Figure 9 showed that the fiber degradation via the hydrolysis rate constant $k_{\text{hyd},\text{ndf}}$ explained
 522 largely most of the variation of s_{ac} over the fermentation for control with a constant
 523 contribution higher than 60% over time. When increasing the dose of AT, the influence of
 524 $k_{\text{hyd},\text{ndf}}$ largely decreased while it was still the most influential IP. Its influence over time
 525 varied from 29 to 42% for low AT treatment and from 26 to 37% for high AT treatment.
 526

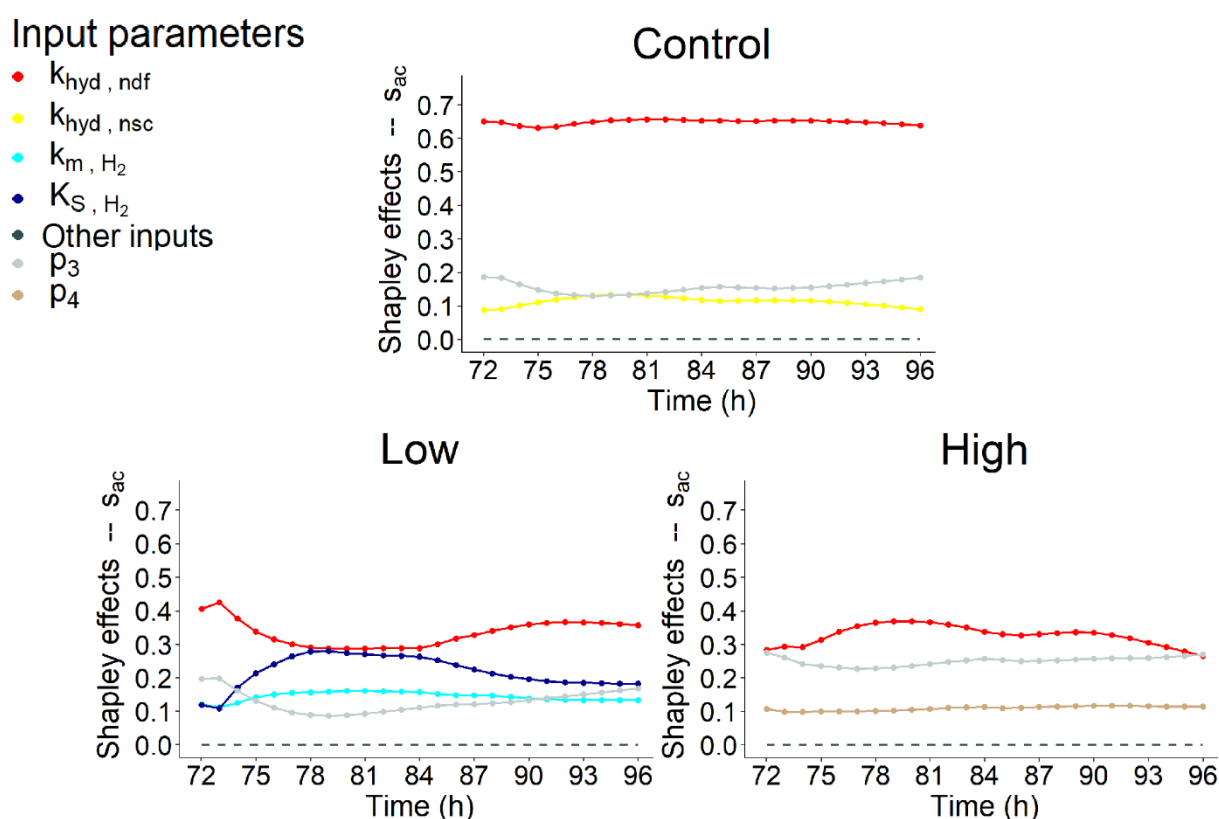


Figure 9. Shapley effects of the influential input parameters (i.e; parameters with a contribution higher than 10% for at least one time step) over time (h) computed for the 4th day of simulation of the acetate concentration (s_{ac} , mol/L) for the 3 dietary scenarios (control: 0% of *Asparagopsis taxiformis*, low treatment: 0.25% of *Asparagopsis taxiformis* and high treatment: 0.50% of *Asparagopsis taxiformis*).

527
 528 The other influential IPs for Control were p_3 , which was the intercept of the factor modeling
 529 the flux allocation from glucose utilization to acetate production in the rumen fermentation
 530 (λ_1), and $k_{\text{hyd},\text{nsc}}$, which was associated with the degradation of non-fiber compounds (Sh_{p_3}

531 and $Sh_{k_{\text{hyd},\text{nsc}}}$ varying from 13 to 19%). The IP $k_{\text{hyd},\text{nsc}}$ was non-influential for AT treatments.
532 Whereas, p_3 was associated with a non-negligible influence (< 20%) for low AT treatment,
533 while it was more important (Sh_{p_3} varying from 23 to 27%) for high AT treatment, which was
534 similar to $k_{\text{hyd},\text{ndf}}$ contribution from 72 to 74h and 93 to 96 h.
535 The microbial group of hydrogen utilizers, via the Monod constant K_{S,H_2} and the maximum
536 specific utilization rate constant k_{m,H_2} , contributed to s_{ac} variability for low AT treatment. This
537 influence was mainly due to K_{S,H_2} , being the second most influential IP from $t = 74\text{h}$ to the
538 end of the fermentation with a contribution varying from 17 to 27% over this period of time.
539 k_{m,H_2} was associated with a low contribution varying from 11 to 16% over the fermentation.
540 The factor λ_1 was also represented via its slope p_4 with a constant low contribution (c.a. 10%)
541 to s_{ac} variability over time for high AT treatment.

542 **3.2.1.3. Butyrate concentration**

543 Similarly to s_{ac} , the fiber degradation via the hydrolysis rate constant $k_{\text{hyd},\text{ndf}}$ was the most
544 influential IP to s_{bu} variability over the fermentation for control and AT treatments (Figure
545 10). Its influence increased when increasing the dose of AT, varying from 34 to 42% for control,
546 from 34 to 43% for low AT treatment and from 54 to 62% for high AT treatment over time.
547

Input parameters

- $k_{\text{hyd}, \text{ndf}}$
- $k_{\text{hyd}, \text{nsc}}$
- k_{m, H_2}
- K_{S, H_2}
- Other inputs
- p_3
- p_5

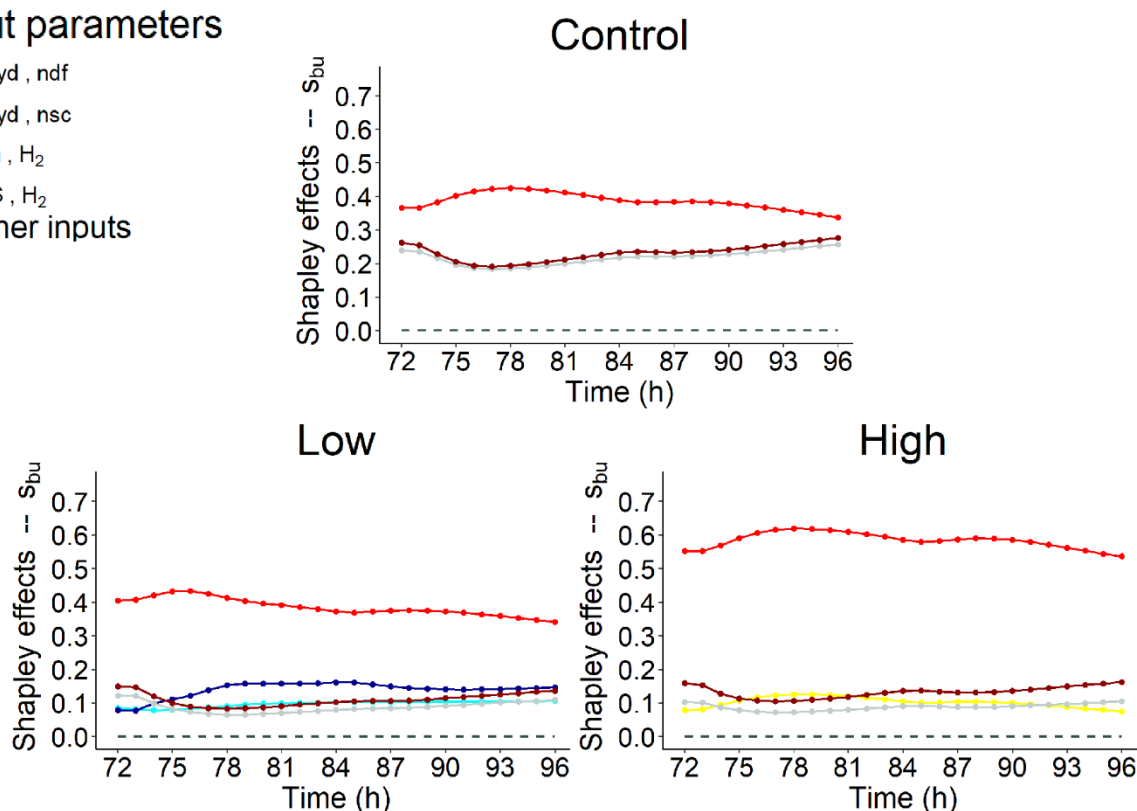


Figure 10. Shapley effects of the influential input parameters (i.e; parameters with a contribution higher than 10% for at least one time step) over time (h) computed for the 4th day of simulation of the butyrate concentration (s_{bu} , mol/L) for the 3 dietary scenarios (control: 0% of *Asparagopsis taxiformis*, low treatment: 0.25% of *Asparagopsis taxiformis* and high treatment: 0.50% of *Asparagopsis taxiformis*).

548
 549 Intercepts of the factors modeling the flux allocation from glucose utilization to acetate and
 550 propionate production in the rumen fermentation (p_3 associated with λ_1 and p_5 associated
 551 with λ_2 , respectively) were the other influential IPs for the 3 dietary scenarios with a similar
 552 contribution over time. The contribution of p_3 and p_5 to s_{bu} variability decreased when
 553 increasing the dose of AT. The contribution of p_3 and p_5 varied from c.a. 18 to 28% for control,
 554 6 to 15% for low AT treatment and 7 to 16% for high AT treatment, respectively.
 555 The microbial group of hydrogen utilizers, via the Monod constant K_{S, H_2} and the maximum
 556 specific utilization rate constant k_{m, H_2} , slightly contributed to s_{bu} variability of the low AT
 557 treatment, similarly to s_{ac} . The contribution of k_{m, H_2} over the fermentation was low (c.a.
 558 10%), while the contribution of K_{S, H_2} was higher, explaining a maximum of 16% of the
 559 variation of s_{bu} (second most influential IP).
 560 The non-fiber degradation via the hydrolysis rate constant $k_{\text{hyd}, \text{nsc}}$ slightly contributed (c.a.
 561 10%) to s_{bu} variability over time of the high AT treatment.

562

3.2.1.4. Propionate concentration

563 The variation of s_{pr} for the 3 dietary scenarios was mainly due to the contributions of 3 IPs
564 (Figure 11).

565

Input parameters

- $k_{hyd, ndf}$
- $k_{hyd, nsc}$
- Other inputs
- p_5

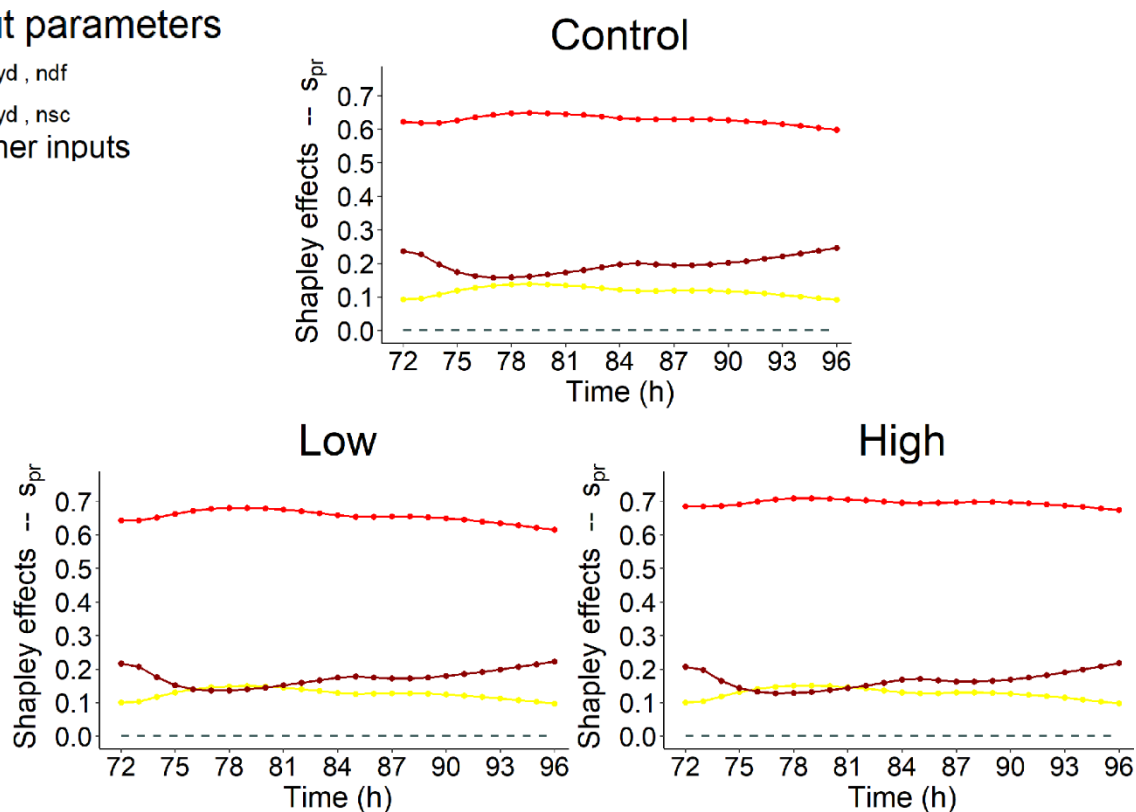


Figure 11. Shapley effects of the influential input parameters (i.e; parameters with a contribution higher than 10% for at least one time step) over time (h) computed for the 4th day of simulation of the propionate concentration (s_{pr} , mol/L) for the 3 dietary scenarios (control: 0% of *Asparagopsis taxiformis*, low treatment: 0.25% of *Asparagopsis taxiformis* and high treatment: 0.50% of *Asparagopsis taxiformis*).

566

567 This result was different from those obtained for the other output variables where new
568 influential IPs were highlighted from a dietary scenario to another. Similarly to s_{ac} and s_{bu} ,
569 the fiber degradation via the hydrolysis rate constant $k_{hyd, ndf}$ was the most influential IP to
570 s_{pr} variability over the fermentation for control and AT treatments. Its influence increased
571 when increasing the dose of AT, varying from 60 to 65% for control, from 61 to 68% for low
572 AT treatment and from 67 to 71% for high AT treatment over time.

573 The other influential IPs were, by order of contribution, the intercept of the factor modeling
574 the flux allocation from glucose utilization to propionate production in the rumen
575 fermentation (p_5 associated with λ_2) and the non-fiber degradation IP $k_{hyd, nsc}$. The
576 contribution of p_5 slightly decreased when increasing the dose of AT with an average
577 contribution over time of 20% for control, 17% for low AT and 16% for high AT. Whereas, the
578 contribution of $k_{hyd, nsc}$ was similar between the 3 dietary scenarios.

579 **3.2.2. Full and independent Sobol indices**

580 Similarly to the Shapley effects, the full and independent Sobol indices of the 16 IPs were
581 computed over time, considering the 4th day of simulation, for the 4 output variables and 3
582 dietary scenarios studied. These indices were computed in addition to the Shapley effects for
583 identifying the nature of the contribution of the IPs to output variable variation. The
584 computational time for one dietary scenario was of 5h using the MESO@LR-Platform.

585 Since the model is associated with independent IPs, the difference between T_i^{full} and T_i^{ind} was
586 systematically close to 0 for all the IPs, output variables and dietary scenarios studied,
587 indicating that the contribution of IPs to output variable variation were not due to the
588 dependence or correlation between IPs.

589 **3.2.2.1. Rate of methane production**

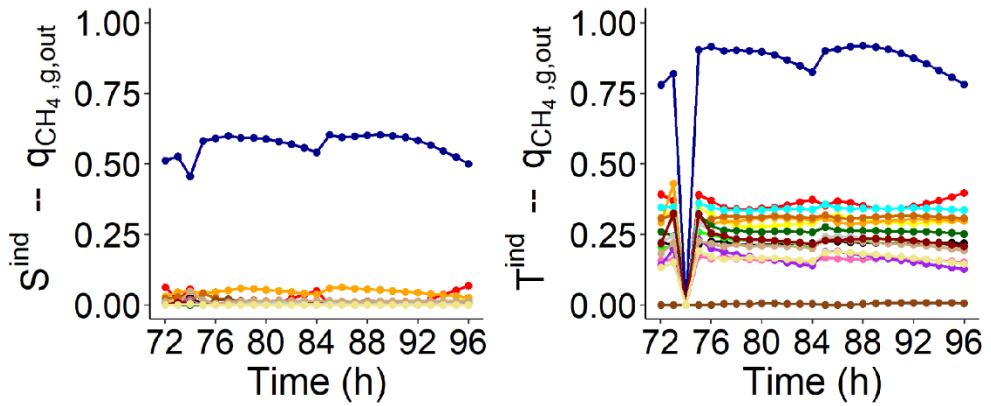
590 The full and independent Sobol indices were displayed only for $q_{\text{CH}_4,\text{g,out}}$ (mol/h) (Figure 12).

591

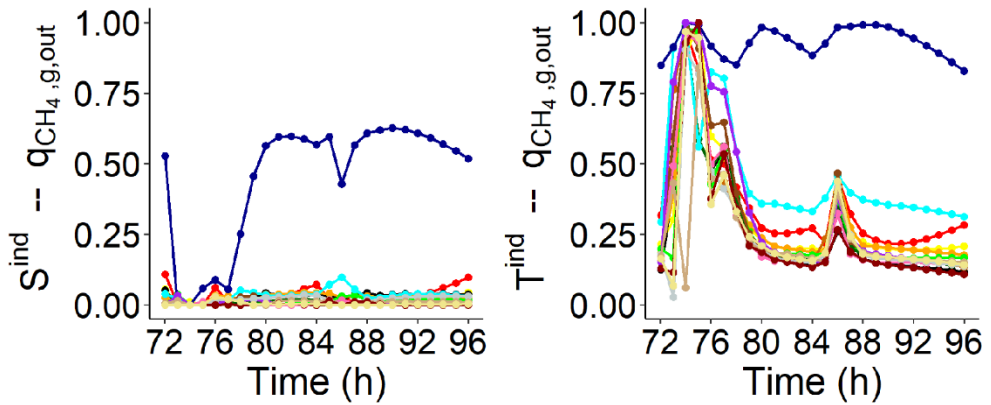
Input parameters

- k_{br}
- $k_{hyd, ndf}$
- $k_{hyd, nsc}$
- $k_{hyd, pro}$
- k_m, aa
- k_m, H_2
- k_m, su
- K_S, aa
- K_S, H_2
- K_S, su
- Other inputs
- p_1
- p_2
- p_3
- p_4
- p_5
- p_6

Control



Low



High

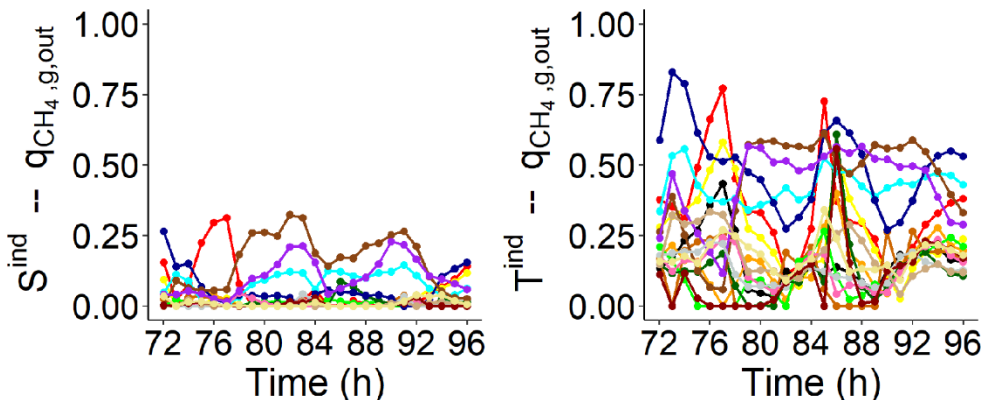


Figure 12. Independent first-order (S^{ind}) and total Sobol indices (T^{ind}) of the input parameters over time (h) computed for the 4th day of simulation of the rate of CH_4 production in gas phase ($q_{CH_4,g,out}$, mol/h) for the 3 dietary scenarios (control: 0% of *Asparagopsis taxiformis*, low treatment: 0.25% of *Asparagopsis taxiformis* and high treatment: 0.50% of *Asparagopsis taxiformis*).

593 The difference between T_i^{ind} and S_i^{ind} over time indicated that interactions between IPs had
594 an important influence on its variation for the control and two AT treatments over the
595 fermentation.

596 For control, the variability of K_{S,H_2} alone had a high contribution on the variation of $q_{CH_4,g,out}$
597 ($S_{K_{S,H_2}}^{\text{ind}}$ varying from 45 to 60%). The contribution of K_{S,H_2} increased over the fermentation
598 when considering its influence via the interactions with other IPs over time ($T_{K_{S,H_2}}^{\text{ind}}$ varying
599 from 78 to 92%). The other IPs did not show any contribution due to their own variability
600 ($S_{i,i \neq K_{S,H_2}}^{\text{ind}}$ c.a. 0). However, their independent total indices indicated that all the IPs interacted
601 with K_{S,H_2} ($T_i^{\text{ind}} \geq 10\%$), except k_{br} with $T_{k_{br}}^{\text{ind}}$ c.a. 0 over the fermentation (which is obvious
602 since there is not bromoform in the control). The influential contribution due to the
603 interactions between IPs was mostly due to interactions of K_{S,H_2} with other IPs such as the
604 fibers degradation ($k_{hyd,ndf}$), the maximum utilization rate of hydrogen utilizers microbial
605 group (k_{m,H_2}), the microbial group of sugars utilizers ($K_{S,su}$ and $k_{m,su}$), the non-fibers
606 degradation ($k_{hyd,nsc}$) and the microbial group of amino acids utilizers ($K_{S,aa}$) with on average
607 $T_{i,i=k_{hyd,ndf},k_{m,H_2},K_{S,su},k_{m,su},k_{hyd,nsc},K_{S,aa}}^{\text{ind}}$ higher than 25% over time.

608 For low AT treatment, K_{S,H_2} was the only IP contributing to $q_{CH_4,g,out}$ variation via its own
609 variability over time, similarly to the control. $S_{K_{S,H_2}}^{\text{ind}}$ varied from 0 to 63% over the fermentation
610 with a contribution lower than 10% from $t = 73$ to $77h$, corresponding to the highest intake
611 activity of the first feed distribution. During this time period, $q_{CH_4,g,out}$ variation was only
612 explained by the interactions between the 16 IPs, with T_i^{ind} higher than 80% for all the IPs for
613 at least one time step during this time period. Similarly to the control, K_{S,H_2} also explained
614 almost all the variability of $q_{CH_4,g,out}$ over the fermentation when considering the contribution
615 via the interactions with other IPs with $T_{K_{S,H_2}}^{\text{ind}}$ varying from 82 to 100% over time. These
616 interactions mainly included k_{m,H_2} and $k_{hyd,ndf}$ with $T_{k_{m,H_2}}^{\text{ind}} = 36\%$ and $T_{k_{hyd,ndf}}^{\text{ind}} = 28\%$ on
617 average over time.

618 For high AT treatment, S_i^{ind} was lower than 32% for all the IPs, indicating that the variation of
619 $q_{CH_4,g,out}$ was mainly due to the interactions between IPs. The IP with the most important
620 individual contribution over the fermentation was $k_{hyd,ndf}$ during the first feed distribution
621 ($S_{k_{hyd,ndf}}^{\text{ind}}$ varying from 22 to 31% from $t = 75$ to $77h$) and at the end of the fermentation
622 ($S_{k_{hyd,ndf}}^{\text{ind}} = 14\%$ at $t = 96h$). Then, the contribution of other IPs such as k_{br} ($S_{k_{br}}^{\text{ind}}$ varying from
623 14 to 32%), p_2 ($S_{p_2}^{\text{ind}}$ varying from 4 to 23%) and k_{m,H_2} ($S_{k_{m,H_2}}^{\text{ind}}$ varying from 3 to 14%) was low
624 in the middle of fermentation from $t = 78$ to $92h$. Also, K_{S,H_2} showed the most important
625 contribution at the beginning and end of the fermentation with $S_{K_{S,H_2}}^{\text{ind}} = 26$ and 15% at $t =$
626 72 and $96h$, respectively. When considering the interactions between IPs, their contribution
627 increased significantly. All the IPs showed a non-negligible contribution ($> 20\%$) for at least
628 one time step, indicating that the 16 IPs were considered in the interactions contributing to
629 $q_{CH_4,g,out}$ variation. IP K_{S,H_2} contributed the most via its interactions with an average

630 difference between $T_{K_{S,H_2}}^{ind}$ and $S_{K_{S,H_2}}^{ind}$ over time of 42%. IP k_{m,H_2} also showed an important
631 contribution throughout the fermentation via the interactions with other IPs with an average
632 constant contribution of 34% over time. The third and fourth IPs contributed the most via the
633 interactions were p_2 and k_{br} , respectively, with on average $T_{p_2}^{ind} - S_{p_2}^{ind} = 33\%$ and $T_{k_{br}}^{ind} -$
634 $S_{k_{br}}^{ind} = 28\%$ over time. These contributions were more important in the middle of
635 fermentation from $t = 78$ to 92 h. Finally, $k_{hyd,ndf}$ and $k_{hyd,nsc}$ also showed a non-negligible
636 contribution via the interactions with on average $T_{k_{hyd,ndf}}^{ind} - S_{k_{hyd,ndf}}^{ind} = 28\%$ and
637 $T_{k_{hyd,nsc}}^{ind} - S_{k_{hyd,nsc}}^{ind} = 24\%$ over time.

638 3.2.2.2. Volatile fatty acids concentration

639 For VFA concentrations (s_{ac} , s_{bu} and s_{pr} , mol/L), the contribution of the interactions between
640 IPs to their variation was lower than 20% (i.e. $T_i^{ind} - S_i^{ind} \leq 20\%$) for the 3 dietary scenarios
641 studied, except for p_5 which described the fraction of glucose utilized to produce propionate
642 and showed a strong influence on s_{ac} , s_{bu} and s_{pr} variation of the control with a maximum
643 contribution of 60, 38 and 29%, respectively. For these 3 variables, the maximum contribution
644 of p_5 via the interactions was reached at the end of the fermentation. Also, the interactions
645 between k_{m,H_2} and other IPs showed a contribution of 24% and 19% to s_{ac} variation for low
646 and high AT treatments, respectively.

647 3.3. Uncertainty analysis

648 Similarly to the full and independent Sobol indices, the uncertainty analysis of simulations
649 computed for estimating the Shapley effects was displayed only for $q_{CH_4,g,out}$. Simulations of
650 VFA used for estimating the Shapley effects were associated with a low variability with a
651 maximum CV of 0.08, 0.12 and 0.09 for s_{ac} , s_{bu} and s_{pr} , respectively.
652 Figure 13 displays the median and quantiles 10% and 90% over time of $q_{CH_4,g,out}$ simulations
653 computed using the IP sampling matrix and the calculated Shapley effects of the 3 dietary
654 scenarios.
655

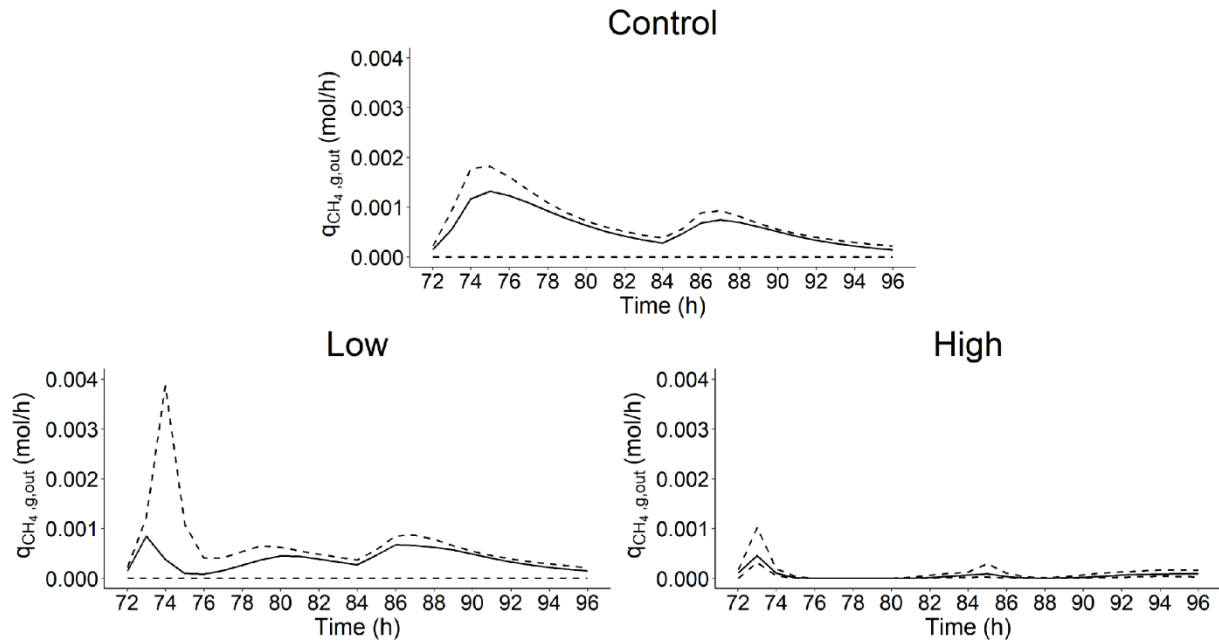


Figure 13. Median and 0.1 and 0.9 quantiles of the rate of methane production in gas phase ($q_{CH_4,g,out}$, mol/h) over time (h) computed from the simulations used to calculate the Shapley effects for the 3 dietary scenarios (control: 0% of *Asparagopsis taxiformis*, low treatment: 0.25% of *Asparagopsis taxiformis* and high treatment: 0.50% of *Asparagopsis taxiformis*).

656

657 When not considering the 10% more extreme simulations, the CV highlighted that $q_{CH_4,g,out}$
658 simulations showed a lower variability for low and high AT treatments with a median CV of
659 0.74 and 0.59, respectively. Whereas, the control showed a median CV of 0.78.

660 Moreover, Figure 14 highlighted that $q_{CH_4,g,out}$ variability varied over time and that this
661 variability was related to the dynamic of DMI (g/h).

662

663

664

665

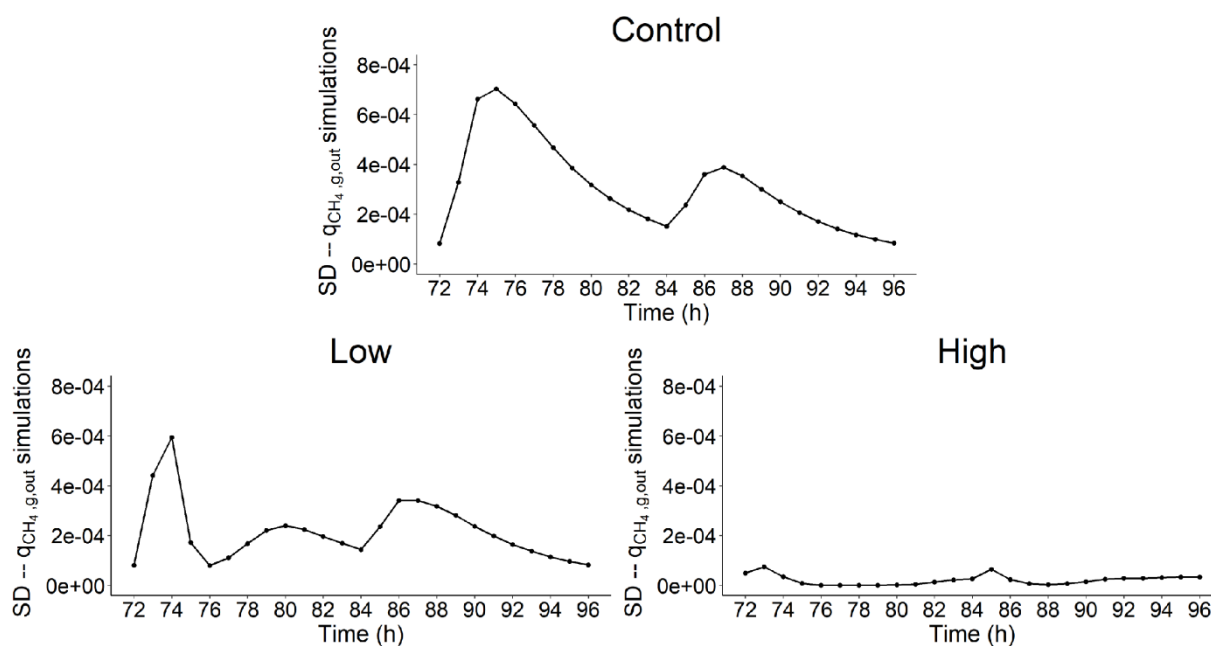


Figure 14. Standard deviation of the simulations of rate of methane production in gas phase ($q_{CH_4,g,out}$, mol/h) over time (h) used to calculate the Shapley effects for the 3 dietary scenarios (control: 0% of *Asparagopsis taxiformis*, low treatment: 0.25% of *Asparagopsis taxiformis* and high treatment: 0.50% of *Asparagopsis taxiformis*).

666

667 The time periods associated with the highest intake activity (represented by the level of decay
668 of the curve of Figure 2) were between 72 and 78h for the first feed distribution and 84 and
669 90h for the second feed distribution. The first feed distribution time period was systematically
670 associated with the highest variability of $q_{CH_4,g,out}$ simulations with a maximum SD of 7e-04
671 mol/h at $t = 75h$, 6e-04 mol/h at $t = 74h$ and 7e-05 mol/h at $t = 73h$ for control, and low and
672 high AT treatments, respectively. This feed distribution represented 70% of the total DM. The
673 second feed distribution, representing 30% of the total DM, was also associated with an
674 important variability of $q_{CH_4,g,out}$ simulations for the 3 dietary scenarios.

675 4. Discussion

676 4.1. Analysis of the simulations of the mechanistic model

677 4.1.1. Comparison with *in vitro* and *in vivo* studies

678 CH₄ reductions between AT treatments obtained with the mechanistic model were lower than
679 those reported in *in vitro* and *in vivo* studies.

680 Chagas et al. (2019) indicated that the inclusion of AT (10 g/kg OM) decreased predicted *in*
681 *vivo* CH₄ production (mL/g DM) of 99% under *in vitro* condition. Whereas, the RUSITEC of
682 Roque et al. (2019) and the *in vitro* study of Romero et al. (2023b) reported reductions of CH₄

683 production (mL/g OM and mL, respectively) of 95% (with a 5% OM dose) and 97% (with a 2%
684 DM dose), respectively.

685 Under *in vivo* conditions, Roque et al. (2021) tested AT doses similar to our simulations. This
686 work reported *in vivo* CH₄ production (g/d) reduction of 32.7 and 51.9% between control, and
687 low and high AT treatments, respectively. The model simulated a lower reduction for low AT
688 treatment and a higher reduction for high AT treatment.

689 These results highlighted that some interactions occurring during the fermentation are not
690 represented in the model (e.g. forage wall content might inhibit the effect of AT). Improving
691 the model involves a finer representation of the interactions between feed characteristics and
692 fermentation as discussed by Bannink et al. (2016).

693 **4.1.2. Analysis of the behavior of VFA proportions**

694 The behavior of VFA proportions dynamic between AT treatments simulated with the models
695 was similar to that of *in vitro* studies. In Chagas et al. (2019), the AT treatment was associated
696 with lower molar proportion of acetate (- 75%) and higher molar proportions of propionate
697 and butyrate (+ 38% and + 47%, respectively). Moreover, the increase of the propionate to
698 acetate ratio was highlighted in Roque et al. (2019) and Romero et al. (2023b). This highlights
699 that the VFA dynamic behavior between AT treatment simulated by the model was consistent
700 with the *in vitro* experiments.

701 **4.2. Sensitivity analysis**

702 **4.2.1. General contribution of the input parameters**

703 **4.2.1.1. Rate of methane production**

704 For the control and low AT treatment, all the variation of $q_{\text{CH}_4, \text{g, out}}$ were explained by the
705 action of the microbial group of hydrogen utilizers represented by the Monod constant $K_{\text{S, H}_2}$.
706 The dynamic of the impact of this microbial group was constant over time and slightly followed
707 the dynamic of DMI.

708 Among all the polymer components describing the feed intake, microbes degrading the fibers
709 with the kinetic $k_{\text{hyd, ndf}}$ explained also a very low part of $q_{\text{CH}_4, \text{g, out}}$ variation. It was also
710 associated with a constant dynamic, following the dynamic of DMI.

711 The comparison of our results with the results of previous SA conducted on mechanistic
712 models of rumen fermentation is not straightforward given the specific model structures and
713 their mathematical formulation. Consequently, the model structure, and the variables and
714 parameters considered in these models are different from those used in our representation,
715 except for Merk et al. (2023) which conducted its SA on an adapted version of the model of
716 Muñoz-Tamayo et al. (2021). However, considering our results in relation to those obtained
717 in previous studies provides useful information to improve our knowledge of the whole
718 picture of the rumen fermentation.

719 When no dose of AT was considered, Merk et al. (2023) also highlighted the impact of fibers
720 degradation component on CH₄ production variation via the initial neutral detergent fiber
721 concentration and $k_{\text{hyd,ndf}}$. This is the initial condition of neutral detergent fiber that was
722 largely associated with the highest contribution (= 43%) to CH₄ production variation. Its other
723 influential IP for the control was related to the flux allocation parameter from glucose
724 utilization to propionate production (λ_2). This last IP was not considered in our SA as we
725 modified the flux allocation parameters in our model version.

726 The low AT treatment highlighted the low participation of IPs describing the kinetic of
727 bromoform utilization (k_{br}) and the direct effect of bromoform on methanogenesis (p_2) to
728 the variability of $q_{\text{CH}_4,\text{g,out}}$, suggesting that the AT dose was too low to highlight a shift in the
729 factors associated to microbial pathways impacting CH₄ production.

730 This shift was highlighted for high AT treatment. k_{br} and p_2 were associated with a high impact
731 on CH₄ production in the middle of the fermentation, replacing a part of the variability
732 explained by the hydrogen utilizers microbial group. However, the impact of $K_{\text{S,H}_2}$ was still
733 important over time, especially at the beginning and at the end of the fermentation. Other IPs
734 associated with the direct (p_1) or indirect (p_4 , p_5 and p_6) effect of bromoform on the
735 fermentations were associated with a low influence on $q_{\text{CH}_4,\text{g,out}}$ variation. This work
736 highlighted that the use of AT to mitigate CH₄ production led to a shift in the factors associated
737 to microbial pathways of the rumen fermentation impacting the CH₄ production.

738 In presence of a dose of AT (included at a 5% inclusion rate), the high impact of IPs associated
739 with bromoform concentration and the factor I_{br} on CH₄ production variation was also
740 highlighted in Merk et al. (2023). The initial bromoform concentration and p_1 showed the
741 highest contributions (= 46%) to CH₄ production variation. This study also mentioned the low
742 but non-negligible impact (c.a. 10%) of IPs related to methanogen abundance, total microbial
743 concentration and hydrogen utilizers microbial group represented by $k_{\text{m,H}_2}$. This last IP
744 showed also an influence on $q_{\text{CH}_4,\text{g,out}}$ variation for high AT treatment in our work. Therefore,
745 Merk et al. (2023) also identified a shift in the key factors driving CH₄ production variation in
746 presence of AT.

747 For other references, the comparison of SA results is only valid for the control as other models
748 did not consider AT treatments. Huhtanen et al. (2015) concluded that IPs associated with
749 degradation kinetics of neutral detergent fiber had a strong influence on CH₄ predictions of
750 Karoline. This factor was also identified as influential in our work but was not associated with
751 a high influence. Fat and the degradation of starch and insoluble protein were the other
752 factors associated with an influence on CH₄ production. Whereas, van Lingen et al. (2019)
753 highlighted that IPs associated with the fractional passage rate for the solid and fluid fractions
754 in the rumen and NADH oxidation rate explained 86% of CH₄ predictions variation of a
755 modified version of the Dijkstra model. Our model does not include the different passage rates
756 between solid and liquid fractions. Finally, Dougherty et al. (2017) found that influential IPs
757 on daily CH₄ production predicted with the AusBeef model were associated with ruminal
758 hydrogen balance and VFA production.

759

4.2.1.2. Volatile fatty acids concentration

760 VFA concentration variation were highly impacted by fibers degradation represented by the
761 kinetic $k_{\text{hyd,ndf}}$ for the control and two AT treatments. $k_{\text{hyd,ndf}}$ was always associated with
762 the highest contribution for s_{ac} , s_{bu} and s_{pr} and the 3 dietary scenarios studied. This
763 contribution was very high (> 50%) for s_{ac} control, s_{bu} high AT treatment and s_{pr} . While, it
764 was intermediate (between 30 and 40% over the fermentation) for s_{ac} low and high AT
765 treatments, and s_{bu} control and low AT treatment. The dynamic of this influence was globally
766 constant over time slightly following the dynamic of DMI, except for s_{ac} low AT treatment
767 which showed a decrease during the first feed distribution. This result was expected as fiber
768 hydrolysis is the limiting step of the fermentation and VFA proportion. Morales et al., (2021)
769 studied the sensitivity of 19 IPs on VFA concentration predicted with Molly. It found that the
770 intercept used for rumen pH prediction was the only influential IP, explaining more than 79%
771 of the variation of acetate, butyrate and propionate concentration predictions of Molly. In this
772 study this result was expected as Molly is a whole animal model, which was not the case of
773 our model. No IPs related to rumen pH were considered in our SA, explaining that the selection
774 of this component was not possible in our case.

775 Hydrogen utilizers microbial group slightly impacted (< 30%) the variation of s_{ac} and s_{bu} for
776 low AT treatment with the 2 IPs representing this group ($K_{\text{S,H}_2}$ and $k_{\text{m,H}_2}$). The influence of
777 these IPs was increasing at the beginning of the fermentation, constant in the middle of the
778 fermentation and decreasing at the end of the fermentation.

779 No shift of the factors associated to microbial pathways impacting VFA production was
780 highlighted when increasing the dose of AT. Moreover, IPs related to the direct effect of
781 bromoform on the fermentation (p_1 and p_2) did not contribute to VFA concentration variation.
782 This suggests that under the conditions evaluated AT had no impact on the biological
783 mechanisms responsible for VFA production in contrast with the one responsible for CH₄
784 production. However, AT supply does have an indirect effect on VFA production to its effect
785 on the lambdas and a variation was observed when considering the molar proportions of VFA
786 (Figure 7).

787 Furthermore, IPs associated with the functions describing the indirect effect of bromoform on
788 rumen fermentation and quantifying reactions driving flux allocation from glucose utilization
789 to acetate (λ_1 associated with p_3 and p_4) and propionate (λ_2 associated with p_5 and p_6)
790 production showed a low impact on VFA concentration variation under our conditions. IP p_3
791 was associated with an impact on s_{ac} and s_{bu} variation. This impact was highlighted for the
792 control and two AT treatments studied with a contribution decreasing at the beginning of the
793 fermentation and then increasing over time lower than 20% for control and low AT treatment
794 and of c.a. 25% for high AT treatment for s_{ac} . Whereas, the contribution over time was more
795 important for the control (c.a. 25%) than for the 2 AT treatments (<20%) for s_{bu} with the same
796 dynamic. p_4 , the negative slope of λ_1 , slightly impacted s_{ac} variation of high AT treatment
797 with a constant dynamic. Regarding λ_2 , p_5 slightly impacted (<30%) s_{bu} and s_{pr} variation over
798 the fermentation for the 3 dietary scenarios with a dynamic slightly decreasing at the

799 beginning of the fermentation and then increasing over time, similarly to p_3 . The positive
800 slope p_6 did not contribute to VFA concentration variation.

801 **4.2.2. Contribution of the interactions between the input** 802 **parameters**

803 In addition to the Shapley effects, full and independent Sobol indices allowed us to investigate
804 if the influential IPs contributed through their own variability or through the variability
805 generated by their dependence/correlation and/or their interactions with other IPs. This step
806 was done as an academic exercise since, by construction, the model does not have
807 dependency between IPs. However, the methodology here illustrated can be useful to address
808 the dependency aspects in future model extensions.

809 **4.2.2.1. Rate of methane production**

810 First-order and total independent Sobol indices highlighted that interactions between IPs
811 played an important role in the contribution of the IPs to $q_{\text{CH}_4,\text{g,out}}$ variation for the control
812 and AT treatments. This contribution was higher for AT treatments than for the control, with
813 the highest contribution for low AT treatment. Merk et al. (2023) also identified the
814 importance of the contribution due to the interactions between IPs for the AT treatment.
815 However, no impact of the interactions was highlighted for the control.

816 The interactions between hydrogen utilizers microbial group via $K_{\text{S,H}_2}$ and the other factors
817 associated to microbial pathways of the rumen fermentation considered had an intermediate
818 impact (~25%) on $q_{\text{CH}_4,\text{g,out}}$ variation for the 3 dietary scenarios considered. Most of the time,
819 these interactions included all the IPs, except k_{br} for the control.

820 The inclusion of all the IPs in the interactions impacting $q_{\text{CH}_4,\text{g,out}}$ variation suggests that the
821 model should be improved to better characterize the interactions. The incorporation of
822 microbial genomic knowledge is expected to improve the representation of rumen microbial
823 fermentation in mathematical models (Davoudkhani et al., 2024; Muñoz-Tamayo et al., 2023).
824 The first feed distribution of the low AT treatment showed that the variation of $q_{\text{CH}_4,\text{g,out}}$ can
825 also be only impacted by the interactions between IPs, highlighting the importance of
826 quantifying the interactions between IPs in SA approaches used.

827 **4.2.2.2. Volatile fatty acids concentration**

828 The contribution due to the interactions was low for VFA concentration variation. Only p_5 , the
829 intercept of λ_2 which is related to propionate production, showed a high contribution via the
830 interactions to VFA concentration variation for control.

831 Finally, the interactions did not affect the dynamic of the contribution over the fermentation
832 for $q_{\text{CH}_4,\text{g,out}}$ and VFA concentrations.

833 **4.3. Uncertainty analysis**

834 The uncertainty of $q_{\text{CH}_4,\text{g,out}}$ and VFA concentration simulations used to compute the Shapley
835 effects was assessed by studying the variability over time of these simulations.

836 **4.3.1. Rate of methane production**

837 The simulations of $q_{\text{CH}_4,\text{g,out}}$ computed by exploring the variability of 6 factors associated to
838 microbial pathways of the rumen fermentation (fiber carbohydrates, non-fiber carbohydrates,
839 proteins, glucose utilizers, amino acids utilizers, hydrogen utilizers) and 4 factors of the effect
840 of bromoform on the fermentation (s_{br} , I_{br} , λ_1 and λ_2) showed a high range of variation for
841 the 3 dietary scenarios.

842 SA results indicated that the variability of $q_{\text{CH}_4,\text{g,out}}$ simulations was only explained by the
843 variation of hydrogen utilizers microbial group via $K_{\text{S,H}_2}$ (alone and in interaction with other
844 factors) for control and low AT treatment. Whereas, the variability of $K_{\text{S,H}_2}$ explained an
845 important part, but also with the variability of other factors, of $q_{\text{CH}_4,\text{g,out}}$ simulation variability
846 for high AT treatment. This suggests that reducing uncertainty associated with $q_{\text{CH}_4,\text{g,out}}$
847 predictions involves to reduce the uncertainty of IPs describing the activity of the hydrogen
848 utilizers microbial group. A way to achieve that is to increase the information available for
849 estimating the variability of parameters describing this microbial group, involving an
850 improvement of our knowledge of it. Finally, when comparing control and AT treatments,
851 $q_{\text{CH}_4,\text{g,out}}$ simulation variability was more important for the control than for low and high AT
852 treatments. This indicates that the shift and increase of factors explaining the variation of
853 $q_{\text{CH}_4,\text{g,out}}$ did not lead to an increase of simulation variability, especially for high AT treatment.
854 Merk et al., (2023) found a different result, computing a CV of 0.23 against 1.22 for simulations
855 associated with control and AT treatment, respectively. However, the range of variation of
856 IPs explored in our study led to outlier simulation for AT treatments. For instance, an IP
857 simulation scenario led to $q_{\text{CH}_4,\text{g,out}}$ values of 96 and 0.07 mol/h at $t = 74$ and 73h for low and
858 high AT treatments, respectively. These outliers were not identified for the control. This
859 suggests that some of the range of variation explored for $K_{\text{S,H}_2}$, $k_{\text{m,H}_2}$, p_2 and k_{br} was not
860 appropriate when considering AT treatments.

861 The dynamic of simulation variability was related to the dynamic of DMI, increasing during the
862 high intake activity period of both feed distributions and decreasing at the end of it. The
863 highest period of variability was associated with the first feed distribution, which
864 corresponded to 70% of the total DM. These results go in line with model developments
865 predicting CH_4 with dynamic data DMI as single predictor (Muñoz-Tamayo et al., 2019, 2022).

866 **4.3.2. Volatile fatty acids concentration**

867 VFA concentrations were associated with much less variability than $q_{\text{CH}_4,\text{g,out}}$, suggesting that
868 these variables are less sensitive to the variation of factors associated to microbial pathways

869 involved in the rumen fermentation analyzed here. Perhaps the consideration of other
870 parameters such as the yield factors would lead to a higher variability of VFA simulations. The
871 variability of these variables was only explained by the individual variability of the kinetic of
872 fibers degradation $k_{\text{hyd,ndf}}$. This suggests that the uncertainty related to $k_{\text{hyd,ndf}}$
873 measurements generates a low uncertainty on VFA concentrations.

874 Similarly to $q_{\text{CH}_4,\text{g,out}}$, the dynamic of the variability of VFA concentration simulations was
875 related to the dynamic of DMI. This variability increased during the high intake activity periods
876 of the first and second feed distributions, with the highest variability reached for the first feed
877 distribution, and decreased at the end of both feed distributions.

878 **4.4. Limitations and perspectives of methods**

879 **4.4.1. Sensitivity analysis approaches**

880 The computation of the Shapley effects allowed to identify the influential and non-influential
881 IPs on the variation of $q_{\text{CH}_4,\text{g,out}}$ and VFA concentration. The use of sensitivity indices for this
882 purpose is becoming increasingly widespread in animal science and our work contributes to
883 the integration of SA in animal modeling. For instance, Merk et al. (2023) conducted local and
884 global SA for identifying key drivers of CH₄ production with or without AT.

885 The main originality of our work is the computation of SI over time, leading to a dynamic
886 interpretation of the impact of key drivers on CH₄ and VFA variation. A second originality is
887 the proposition of an approach allowing to discriminate the nature of the contribution of IPs
888 to output variable variation. Although, considering the contribution due to the
889 dependence/correlation between IPs was not relevant in our case study, this work proposes
890 a first methodology to handle this kind of contribution in the case of development of more
891 complex models involving dependent or correlated IPs.

892 Our study used simulation conditions based on RUSITEC *in vitro* experiments. Future work can
893 use our SA framework to identify useful sampling times and experimental conditions to
894 provide informative data for model refinement in the context of optimal experiment design
895 for parameter estimation.

896 Regarding our SA results, it is important to mention that they are inherently linked to the
897 representation of the rumen fermentation considered in our case study.

898 **4.4.2. Uncertainty analysis**

899 The *in silico* framework used for the SA shows that the factors associated to microbial
900 pathways modeled in our case study mainly impacted CH₄ prediction uncertainty. This
901 suggests that an improvement in the range of variation of parameters associated with the
902 methanogenesis should lead to a reduction of the uncertainty associated with model
903 predictions. The high AT treatment also showed that the parameters associated with the
904 bromoform effect on the fermentation impacted negatively the prediction uncertainty. These

905 suggestions should be carefully interpreted because limited by the low information available
906 on the numerical values of parameters of the equations representing the rumen fermentation.

907 **5. Conclusions**

908 A dynamic sensitivity analysis of a model describing the effect of bromoform (via *Asparagopsis*
909 *taxiformis*) on rumen fermentation under *in vitro* continuous condition was conducted. The
910 hydrogen utilizers microbial group was identified as the key factor explaining methane
911 variation over time for the control and low dose treatments. This factor was associated with
912 the microbial methanogenesis. The high AT dose treatment showed a shift in the factors
913 associated to microbial pathways explaining methane variation, highlighting the emergence
914 of parameters associated with bromoform concentration and direct effect of bromoform on
915 methanogenesis. The interactions between parameters played a role in these contributions.
916 Moreover, the individual variability of kinetic of fibers degradation explained most of the VFA
917 variation. The uncertainty analysis of simulations computed for SA suggested that reducing
918 the uncertainty of the parameters associated to the kinetics of hydrogen utilizers microbial
919 group should lead to a reduction of model prediction uncertainty. Our work showed that
920 implementing dynamic sensitivity analysis is a promising approach to improve our
921 understanding of mechanisms involved in the rumen fermentation and can help to design
922 optimal experiments assessing methane mitigation strategies.

923 **6. Declarations**

924 **Funding**

925 Paul Blondiaux is funded with a scholarship from the doctoral school ABIES (AgroParisTech,
926 France) and from the INRAE PHASE department (France).

927 **Availability of data and material**

928 The scripts for the model simulation and SA are available at Blondiaux (2024)

929 **Competing interests**

930 The authors declare that they comply with the PCI rule of having no financial conflicts of
931 interest in relation to the content of the article. The authors declare the following non-
932 financial conflict of interest: Rafael Muñoz-Tamayo is member of the managing board of PCI
933 Animal Science and recommender of PCI Microbiology.

934 **CRedit Author contributions**

935 Paul Blondiaux: Conceptualization, Data curation, Formal Analysis, Investigation,
936 Methodology, Software, Writing – original draft

937 Tristan Senga Kiessé: Conceptualization, Funding acquisition, Methodology, Supervision,
938 Writing – review & editing

939 Maguy Eugène: Conceptualization, Funding acquisition, Methodology, Supervision, Writing –
940 review & editing

941 Rafael Muñoz-Tamayo: Conceptualization, Funding acquisition, Investigation, Methodology,
942 Project administration, Software, Supervision, Writing – review & editing

943 **7. References**

- 944 Aluwong, T., Wuyep, P., Allam, L., 2011. Livestock-environment interactions: Methane
945 emissions from ruminants. *African J. Biotechnol.* 10, 1265–1269.
946 <https://doi.org/10.4314/AJB.V10I8>
- 947 Arndt, C., Hristov, A.N., Price, W.J., McClelland, S.C., Pelaez, A.M., Cueva, S.F., Oh, J., Dijkstra,
948 J., Bannink, A., Bayat, A.R., Crompton, L.A., Eugène, M.A., Enahoro, D., Kebreab, E.,
949 Kreuzer, M., McGee, M., Martin, C., Newbold, C.J., Reynolds, C.K., Schwarm, A.,
950 Shingfield, K.J., Veneman, J.B., Yáñez-Ruiz, D.R., Yu, Z., 2022. Full adoption of the most
951 effective strategies to mitigate methane emissions by ruminants can help meet the 1.5
952 °C target by 2030 but not 2050. *Proc. Natl. Acad. Sci. U. S. A.* 119.
953 <https://doi.org/10.1073/PNAS.2111294119/-/DCSUPPLEMENTAL>
- 954 Baldwin, R.L., Thornley, J.H.M., Beaver, D.E., 1987. Metabolism of the lactating cow: II.
955 Digestive elements of a mechanistic model. *J. Dairy Res.* 54.
956 <https://doi.org/10.1017/s0022029900025231>
- 957 Bannink, A., Kogut, J., Dijkstra, J., France, J., Kebreab, E., Van Vuuren, A.M., Tamminga, S.,
958 2006. Estimation of the stoichiometry of volatile fatty acid production in the rumen of
959 lactating cows. *J. Theor. Biol.* 238, 36–51. <https://doi.org/10.1016/j.jtbi.2005.05.026>
- 960 Bannink, A., van Lingen, H.J., Ellis, J.L., France, J., Dijkstra, J., 2016. The contribution of
961 mathematical modeling to understanding dynamic aspects of rumen metabolism. *Front.*
962 *Microbiol.* 7, 166675. <https://doi.org/10.3389/FMICB.2016.01820/BIBTEX>
- 963 Batstone, D.J., Keller, J., Angelidaki, I., Kalyuzhnyi, S. V., Pavlostathis, S.G., Rozzi, A., Sanders,
964 W.T., Siegrist, H., Vavilin, V.A., 2002. The IWA Anaerobic Digestion Model No 1 (ADM1).
965 *Water Sci. Technol.* 45. <https://doi.org/10.2166/wst.2002.0292>
- 966 Bayat, A.R., Rinne, M., Kuoppala, K., Ahvenjärvi, S., Huhtanen, P., 2011. Ruminant large and
967 small particle kinetics in dairy cows fed primary growth and regrowth grass silages
968 harvested at two stages of growth. *Anim. Feed Sci. Technol.* 165, 51–60.
969 <https://doi.org/10.1016/j.anifeedsci.2011.02.018>
- 970 Beauchemin, K.A., Ungerfeld, E.M., Eckard, R.J., Wang, M., 2020. Review: Fifty years of
971 research on rumen methanogenesis: lessons learned and future challenges for
972 mitigation. *Animal* 14, s2–s16. <https://doi.org/10.1017/S1751731119003100>
- 973 Belanche, A., Newbold, C.J., Lin, W., Stevens, P.R., Kingston-Smith, A.H., 2017. A systems
974 biology approach reveals differences in the dynamics of colonization and degradation of
975 grass vs. Hay by rumen microbes with minor effects of vitamin E supplementation.
976 *Front. Microbiol.* 8, 1–18. <https://doi.org/10.3389/fmicb.2017.01456>
- 977 Benchaar, C., Rivest, J., Pomar, C., Chiquette, J., 1997. Prediction of Methane Production
978 from Dairy Cows Using Existing Mechanistic Models and Regression Equations 1. *J.*
979 *Anim. Sci* 76, 617–627.

- 980 Bertrand looss, A., Da Veiga, S., Janon, A., Pujol, G., contribu-tions from Baptiste Broto, with,
981 Boumhaout, K., Clouvel, L., De-lage, T., El Amri, R., Fruth, J., Gilquin, L., Guillaume, J.,
982 Herin, M., Il Idrissi, M., Le Gratiét, L., Lemaitre, P., Marrel, A., Mey-naoui, A., Nelson,
983 B.L., Monari, F., Oomen, R., Rakovec, O., Ramos, B., Rous-tant, O., Sarazin, G., Song, E.,
984 Staum, J., Sueur, R., Touati, T., Verges, V., Weber, F., 2023. Package “sensitivity” Title
985 Global Sensitivity Analysis of Model Outputs.
- 986 Blondiaux, P., 2024. Implementation of a dynamic sensitivity analysis of a mathematical
987 model describing the effect of the macroalgae *Asparagopsis taxiformis* on rumen
988 fermentation and methane production under in vitro continuous conditions.
989 <https://doi.org/10.5281/ZENODO.12167243>
- 990 Blondiaux, P., Senga Kiessé, T., Eugène, M., Muñoz-Tamayo, R., 2022. 20. Sensitivity analysis
991 of a mechanistic model of the rumen in-vitro fermentation: Study of the impact of 3
992 sampling methods on Sobol indices of accuracy. *Anim. - Sci. Proc.* 13, 532–533.
993 <https://doi.org/10.1016/J.ANSCIP.2022.07.411>
- 994 Castro, J., Gómez, D., Tejada, J., 2009. Polynomial calculation of the Shapley value based on
995 sampling. *Comput. Oper. Res.* 36. <https://doi.org/10.1016/j.cor.2008.04.004>
- 996 Chagas, J.C., Ramin, M., Krizsan, S.J., 2019. In Vitro Evaluation of Different Dietary Methane
997 Mitigation Strategies. *Animals* 9, 1120. <https://doi.org/10.3390/ani9121120>
- 998 Chapoutot, P., Dorléans, M., Sauvart, D., 2010. Études des cinétiques de dégradation dans le
999 rumen des constituants pariétaux des aliments concentrés et coproduits
1000 agroindustriels. *INRAE Prod. Anim.* 23, 285–304.
1001 <https://doi.org/10.20870/PRODUCTIONS-ANIMALES.2010.23.3.3309>
- 1002 CITEPA, 2023. Gaz à effet de serre et polluants atmosphériques. Bilan des émissions en
1003 France de 1990 à 2022.
- 1004 Danfær, A., Huhtanen, P., Udén, P., Sveinbjörnsson, J., Volden, H., 2006. The nordic dairy
1005 cow model, karoline - description. *Nutr. Dig. Util. Farm Anim. Model. Approaches* 383–
1006 406. <https://doi.org/10.1079/9781845930059.0383>
- 1007 Davoudkhani, M., Rubino, F., Creevey, C.J., Ahvenjärvi, S., Bayat, A.R., Tapio, I., Belanche, A.,
1008 Muñoz-Tamayo, R., 2024. Integrating microbial abundance time series with
1009 fermentation dynamics of the rumen microbiome via mathematical modelling. *PLoS*
1010 *One* 19, e0298930. <https://doi.org/10.1371/JOURNAL.PONE.0298930>
- 1011 Dijkstra, J., Neal, H.D.S.C., Beever, D.E., France, J., 1992. Simulation of nutrient digestion,
1012 absorption and outflow in the rumen: Model description. *J. Nutr.* 122.
1013 <https://doi.org/10.1093/jn/122.11.2239>
- 1014 Dougherty, H.C., Kebreab, E., Evered, M., Little, B.A., Ingham, A.B., Nolan, J. V., Hegarty, R.S.,
1015 Pacheco, D., Mcphee, M.J., 2017. The AusBeef model for beef production: II. sensitivity
1016 analysis. *J. Agric. Sci.* 155. <https://doi.org/10.1017/S0021859617000430>
- 1017 Faivre, R., looss, B., Mahévas, S., Makowski, D., Monod, H., 2013. Analyse de sensibilité et
1018 exploration de modèles : Application aux sciences de la nature et de l’environnement
1019 1–352.
- 1020 Fao, 2017. Livestock solutions for climate change.
- 1021 Homma, T., Saltelli, A., 1996. Importance measures in global sensitivity analysis of nonlinear
1022 models. *Reliab. Eng. Syst. Saf.* 52. [https://doi.org/10.1016/0951-8320\(96\)00002-6](https://doi.org/10.1016/0951-8320(96)00002-6)
- 1023 Hristov, A.N., Oh, J., Firkins, J.L., Dijkstra, J., Kebreab, E., Waghorn, G., Makkar, # H P S,
1024 Adesogan, || A T, Yang, ¶ W, Lee, C., Gerber ||, P.J., Henderson ||, B., Tricarico, J.M.,
1025 2013. SPECIAL TOPICS-Mitigation of methane and nitrous oxide emissions from animal
1026 operations: I. A review of enteric methane mitigation options 1. *J. Anim. Sci* 91, 5045–

- 1027 5069. <https://doi.org/10.2527/jas2013-6583>
- 1028 Huhtanen, P., Ramin, M., Udén, P., 2015. Nordic dairy cow model Karoline in predicting
1029 methane emissions: 1. Model description and sensitivity analysis. *Livest. Sci.* 178.
1030 <https://doi.org/10.1016/j.livsci.2015.05.009>
- 1031 looss, B., Lemaître, P., 2015. A review on global sensitivity analysis methods. *Oper. Res.*
1032 *Comput. Sci. Interfaces Ser.* 59, 101–122. [https://doi.org/10.1007/978-1-4899-7547-](https://doi.org/10.1007/978-1-4899-7547-8_5/COVER)
1033 [8_5/COVER](https://doi.org/10.1007/978-1-4899-7547-8_5/COVER)
- 1034 looss, B., Prieur, C., 2019. Shapley effects for sensitivity analysis with correlated inputs:
1035 Comparisons with sobol' indices, numerical estimation and applications. *Int. J.*
1036 *Uncertain. Quantif.* 9.
1037 <https://doi.org/10.1615/Int.J.UncertaintyQuantification.2019028372>
- 1038 IPCC, 2022. IPCC, 2018: Global Warming of 1.5°C. Cambridge University Press.
1039 <https://doi.org/10.1017/9781009157940>
- 1040 Kinley, R.D., De Nys, R., Vucko, M.J., MacHado, L., Tomkins, N.W., 2016. The red macroalgae
1041 *Asparagopsis taxiformis* is a potent natural antimethanogenic that reduces methane
1042 production during in vitro fermentation with rumen fluid. *Anim. Prod. Sci.* 56, 282–289.
1043 <https://doi.org/10.1071/AN15576>
- 1044 Kinley, R.D., Martinez-Fernandez, G., Matthews, M.K., De Nys, R., Magnusson, M., Tomkins,
1045 N.W., 2020. Mitigating the carbon footprint and improving productivity of ruminant
1046 livestock agriculture using a red seaweed.
1047 <https://doi.org/10.1016/j.jclepro.2020.120836>
- 1048 Kucherenko, S., Tarantola, S., Annoni, P., 2012. Estimation of global sensitivity indices for
1049 models with dependent variables. *Comput. Phys. Commun.* 183.
1050 <https://doi.org/10.1016/j.cpc.2011.12.020>
- 1051 Lescoat, P., Sauvant, D., 1995. Development of a mechanistic model for rumen digestion
1052 validated using the duodenal flux of amino acids.
- 1053 Li, X., Norman, H.C., Kinley, R.D., Laurence, M., Wilmot, M., Bender, H., De Nys, R., Tomkins,
1054 N., 2016. *Asparagopsis taxiformis* decreases enteric methane production from sheep.
1055 *Anim. Prod. Sci.* 58, 681–688. <https://doi.org/10.1071/AN15883>
- 1056 Machado, L., Magnusson, M., Paul, N.A., De Nys, R., Tomkins, N., 2014. Effects of Marine and
1057 Freshwater Macroalgae on In Vitro Total Gas and Methane Production. *PLoS One* 9,
1058 e85289. <https://doi.org/10.1371/JOURNAL.PONE.0085289>
- 1059 Machado, L., Magnusson, M., Paul, N.A., Kinley, R., de Nys, R., Tomkins, N., 2016. Dose-
1060 response effects of *Asparagopsis taxiformis* and *Oedogonium* sp. on in vitro
1061 fermentation and methane production. *J. Appl. Phycol.* 28, 1443–1452.
1062 <https://doi.org/10.1007/s10811-015-0639-9>
- 1063 Mara, T.A., Tarantola, S., 2012. Variance-based sensitivity indices for models with dependent
1064 inputs, in: *Reliability Engineering and System Safety*.
1065 <https://doi.org/10.1016/j.ress.2011.08.008>
- 1066 Mara, T.A., Tarantola, S., Annoni, P., 2015. Non-parametric methods for global sensitivity
1067 analysis of model output with dependent inputs. *Environ. Model. Softw.* 72.
1068 <https://doi.org/10.1016/j.envsoft.2015.07.010>
- 1069 Mcgrath, J., Duval, S.M., Tamassia, L.F.M., Kindermann, M., Stemmler, R.T., De Gouvea, V.N.,
1070 Acedo, T.S., Immig, I., Williams, S.N., Celi, P., 2017. Nutritional strategies in ruminants: A
1071 lifetime approach. <https://doi.org/10.1016/j.rvsc.2017.09.011>
- 1072 Merk, K., Link, K.G., Guy, R.D., Hess, M., 2023. Sensitivity analysis of a mechanistic model of
1073 rumen fermentation and methane production by rumen microbiota in the presence of

- 1074 Asparagopsis taxiformis. bioRxiv 2023.11.30.569127.
1075 <https://doi.org/10.1101/2023.11.30.569127>
- 1076 Mills, J.A.N., Crompton, L.A., Ellis, J.L., Dijkstra, J., Bannink, A., Hook, S., Benchaar, C., France,
1077 J., 2014. A dynamic mechanistic model of lactic acid metabolism in the rumen. J. Dairy
1078 Sci. 97, 2398–2414. <https://doi.org/10.3168/JDS.2013-7582>
- 1079 Morales, A.G., Vibart, R.E., Li, M.M., Jonker, A., Pacheco, D., Hanigan, M.D., 2021. Evaluation
1080 of Molly model predictions of ruminal fermentation, nutrient digestion, and
1081 performance by dairy cows consuming ryegrass-based diets. J. Dairy Sci. 104, 9676–
1082 9702. <https://doi.org/10.3168/JDS.2020-19740>
- 1083 Morgavi, D.P., Cantalapiedra-Hijar, G., Eugène, M., Martin, C., Nozière, P., Popova, M.,
1084 Ortigues-Marty, I., Muñoz-Tamayo, R., Ungerfeld, E.M., 2023. Review: Reducing enteric
1085 methane emissions improves energy metabolism in livestock: is the tenet right? animal
1086 17, 100830. <https://doi.org/10.1016/J.ANIMAL.2023.100830>
- 1087 Morgavi, D.P., Forano, E., Martin, C., Newbold, C.J., 2010. Microbial ecosystem and
1088 methanogenesis in ruminants. Animal 4, 1024–1036.
1089 <https://doi.org/10.1017/S1751731110000546>
- 1090 Mosey, F.E., 1983. Mathematical Modelling of the Anaerobic Digestion Process: Regulatory
1091 Mechanisms for the Formation of Short-Chain Volatile Acids from Glucose. Water Sci.
1092 Technol. 15, 209–232. <https://doi.org/10.2166/WST.1983.0168>
- 1093 Muñoz-Tamayo, R., 2020. Implementation of a mathematical model predicting the impact of
1094 Asparagopsis taxiformis supply on in vitro rumen microbial fermentation and methane
1095 production. <https://doi.org/10.5281/ZENODO.11239148>
- 1096 Muñoz-Tamayo, R., Chagas, J.C., Ramin, M., 2021a. Understanding the mechanisms behind
1097 natural bioactive compounds that can potentially reduce methane production in
1098 anaerobic conditions. A case study of Asparagopsis taxiformis. Peer Community Anim.
1099 Sci. 1, 100006. <https://doi.org/10.24072/PCI.ANIMSCI.100006>
- 1100 Muñoz-Tamayo, R., Chagas, J.C., Ramin, M., Krizsan, S.J., 2021b. Modelling the impact of the
1101 macroalgae Asparagopsis taxiformis on rumen microbial fermentation and methane
1102 production. Peer Community J. 1. <https://doi.org/10.24072/pcjournal.11>
- 1103 Muñoz-Tamayo, R., Davoudkhani, M., Fakhri, I., Robles-Rodríguez, C.E., Rubino, F., Creevey,
1104 C.J., Forano, E., 2023. Review: Towards the next-generation models of the rumen
1105 microbiome for enhancing predictive power and guiding sustainable production
1106 strategies. animal 17, 100984. <https://doi.org/10.1016/J.ANIMAL.2023.100984>
- 1107 Muñoz-Tamayo, R., Giger-Reverdin, S., Sauvant, D., 2016. Mechanistic modelling of in vitro
1108 fermentation and methane production by rumen microbiota. Anim. Feed Sci. Technol.
1109 220. <https://doi.org/10.1016/j.anifeedsci.2016.07.005>
- 1110 Muñoz-Tamayo, R., Ramírez Agudelo, J.F., Dewhurst, R.J., Miller, G., Vernon, T., Kettle, H.,
1111 2019. A parsimonious software sensor for estimating the individual dynamic pattern of
1112 methane emissions from cattle. animal 13, 1180–1187.
1113 <https://doi.org/10.1017/S1751731118002550>
- 1114 Muñoz-Tamayo, R., Ruiz, B., Blavy, P., Giger-Reverdin, S., Sauvant, D., Williams, S.R.O.,
1115 Moate, P.J., 2022. Predicting the dynamics of enteric methane emissions based on
1116 intake kinetic patterns in dairy cows fed diets containing either wheat or corn animal-
1117 open space. <https://doi.org/10.1016/j.anopes.2021.100003>
- 1118 Nagorcka, B.N., Gordon, G.L.R., Dynes, R.A., Mcnamara, J.P., France, J., Beever, D.E., 2000.
1119 Towards a more accurate representation of fermentation in mathematical models of
1120 the rumen. Model. Nutr. Util. farm Anim. 37–48.

- 1121 <https://doi.org/10.1079/9780851994499.0037>
- 1122 Owen, A.B., 2014. Sobol' indices and shapley value. SIAM-ASA J. Uncertain. Quantif. 2.
- 1123 <https://doi.org/10.1137/130936233>
- 1124 Pellerin, S., Bamière, L., Angers, D., Béline, F., Benoît, M., Butault, J.-P., Chenu, C., Colnenne-
1125 David, C., de Cara, S., Delame, N., Doreau, M., Dupraz, P., Faverdin, P., Garcia-Launay,
1126 F., Hassouna, M., Hénault, C., Jeuffroy, M.-H., Klumpp, K., Metay, A., Moran, D., Recous,
1127 S., Samson, E., Savini, I., Pardon, L., 2013. QUELLE CONTRIBUTION DE L'AGRICULTURE
1128 FRANÇAISE À LA RÉDUCTION DES ÉMISSIONS DE GAZ À EFFET DE SERRE ? POTENTIEL
1129 D'ATTÉNUATION ET COÛT DE DIX ACTIONS TECHNIQUES Synthèse du rapport de l'
1130 étude réalisée par l'INRA pour le compte de l'ADEME, du MAAF et du M.
- 1131 Puy, A., Piano, S. Lo, Saltelli, A., Levin, S.A., 2022. **sensobol** : An R Package to Compute
1132 Variance-Based Sensitivity Indices. J. Stat. Softw. 102.
1133 <https://doi.org/10.18637/jss.v102.i05>
- 1134 Romero, Pedro, Belanche, A., Jiménez, E., Hueso, R., Ramos-Morales, E., Salwen, J.K.,
1135 Kebreab, E., Yáñez-Ruiz, D.R., 2023. Rumen microbial degradation of bromoform from
1136 red seaweed (*Asparagopsis taxiformis*) and the impact on rumen fermentation and
1137 methanogenic archaea. J. Anim. Sci. Biotechnol. 2023 141 14, 1–15.
1138 <https://doi.org/10.1186/S40104-023-00935-Z>
- 1139 Romero, P., Huang, R., Jiménez, E., Palma-Hidalgo, J.M., Ungerfeld, E.M., Popova, M.,
1140 Morgavi, D.P., Belanche, A., Yáñez-Ruiz, D.R., 2023. Evaluating the effect of phenolic
1141 compounds as hydrogen acceptors when ruminal methanogenesis is inhibited in vitro –
1142 Part 2. Dairy goats. animal 17, 100789. <https://doi.org/10.1016/J.ANIMAL.2023.100789>
- 1143 Roque, B.M., Brooke, C.G., Ladau, J., Polley, T., Marsh, L.J., Najafi, N., Pandey, P., Singh, L.,
1144 Kinley, R., Salwen, J.K., Eloë-Fadrosch, E., Kebreab, E., Hess, M., 2019. Effect of the
1145 macroalgae *Asparagopsis taxiformis* on methane production and rumen microbiome
1146 assemblage. Anim. Microbiome 1:3. <https://doi.org/10.1186/s42523-019-0004-4>
- 1147 Roque, B.M., Venegas, M., Kinley, R.D., De Nys, R., Duarte, T.L., Yang, X., Kebreab, E., 2021.
1148 Red seaweed (*Asparagopsis taxiformis*) supplementation reduces enteric methane by
1149 over 80 percent in beef steers. PLoS One 16, e0247820.
1150 <https://doi.org/10.1371/JOURNAL.PONE.0247820>
- 1151 Saltelli, A., Ratto, M., Andres, T., Campolongo, F., Cariboni, J., Gatelli, D., Saisana, M.,
1152 Tarantola, S., 2008. Global sensitivity analysis: The primer. Glob. Sensit. Anal. Prim. 1–
1153 292. <https://doi.org/10.1002/9780470725184>
- 1154 Saltelli, A., Ratto, M., Tarantola, S., Campolongo, F., 2005. Sensitivity analysis for chemical
1155 models. Chem. Rev. 105, 2811–2827. <https://doi.org/10.1021/CR040659D>
- 1156 Serment, A., Giger-Reverdin, S., Schmidely, P., Dhumez, O., Broudiscou, L.P., Sauvant, D.,
1157 2016. In vitro fermentation of total mixed diets differing in concentrate proportion:
1158 Relative effects of inocula and substrates. J. Sci. Food Agric. 96, 160–168.
1159 <https://doi.org/10.1002/JSFA.7076>
- 1160 Serment, A., Sauvant, D., 2011. A mechanistic model of pH and gas exchanges in the rumen
1161 and its in vitro application. Model. Nutr. Dig. Util. farm Anim. 148–157.
1162 https://doi.org/10.3920/978-90-8686-712-7_16
- 1163 Shapley, L.S., 1953. A Value for n-person Games. Contributions to the Theory of Games. Ann.
1164 Math. Stud. 28.
- 1165 Sobol, I.M., 1993. Sensitivity analysis for non-linear mathematical models. Math. Model.
1166 Comput. Exp. 1.
- 1167 Song, E., Nelson, B.L., Staum, J., 2016. Shapley effects for global sensitivity analysis: Theory

- 1168 and computation. *SIAM-ASA J. Uncertain. Quantif.* 4.
1169 <https://doi.org/10.1137/15M1048070>
- 1170 Stefenoni, H.A., Räisänen, S.E., Cueva, S.F., Wasson, D.E., Lage, C.F.A., Melgar, A., Fetter,
1171 M.E., Smith, P., Hennessy, M., Vecchiarelli, B., Bender, J., Pitta, D., Cantrell, C.L., Yarish,
1172 C., Hristov, A.N., 2021. Effects of the macroalga *Asparagopsis taxiformis* and oregano
1173 leaves on methane emission, rumen fermentation, and lactational performance of dairy
1174 cows. *J. Dairy Sci.* 104, 4157–4173. <https://doi.org/10.3168/JDS.2020-19686>
- 1175 Tedeschi, L.O., Cavalcanti, L.F.L., Fonseca, M.A., Herrero, M., Thornton, P.K., 2014. The
1176 evolution and evaluation of dairy cattle models for predicting milk production: An
1177 agricultural model intercomparison and improvement project (AgMIP) for livestock.
1178 *Anim. Prod. Sci.* 54, 2052–2067. <https://doi.org/10.1071/AN14620>
- 1179 Terry, S.A., Krüger, A.M., Lima, P.M.T., Gruninger, R.J., Abbott, D.W., Beauchemin, K.A.,
1180 2023. Evaluation of Rumen Fermentation and Microbial Adaptation to Three Red
1181 Seaweeds Using the Rumen Simulation Technique. *Anim.* 2023, Vol. 13, Page 1643 13,
1182 1643. <https://doi.org/10.3390/ANI13101643>
- 1183 Torres, M.G., Soriano, R., Peralta, J.J., Alejos, J.I., Sánchez, P., Arias, L., Campos, R.G.,
1184 Almaraz, I., 2020. Challenges of livestock: climate change, animal welfare and
1185 agroforestry. *Large Anim. Rev.* 26, 39–45.
- 1186 van Lingen, H.J., Fadel, J.G., Moraes, L.E., Bannink, A., Dijkstra, J., 2019. Bayesian mechanistic
1187 modeling of thermodynamically controlled volatile fatty acid, hydrogen and methane
1188 production in the bovine rumen. *J. Theor. Biol.* 480.
1189 <https://doi.org/10.1016/j.jtbi.2019.08.008>
- 1190 Xu, C., 2013. Decoupling correlated and uncorrelated parametric uncertainty contributions
1191 for nonlinear models. <https://doi.org/10.1016/j.apm.2013.05.036>
- 1192 Xu, C., Zdzislaw Gertner, G., 2008. Uncertainty and sensitivity analysis for models with
1193 correlated parameters. *Reliab. Eng. Syst. Saf.* 93, 1563–1573.
1194 <https://doi.org/10.1016/j.res.2007.06.003>

1195